

University of Alabama in Huntsville

**LOUIS**

---

Theses

UAH Electronic Theses and Dissertations

---

2010

## Numerical optimization of a liquid propellant settling scenario

Josh Rojahn

Follow this and additional works at: <https://louis.uah.edu/uah-theses>

---

### Recommended Citation

Rojahn, Josh, "Numerical optimization of a liquid propellant settling scenario" (2010). *Theses*. 695.  
<https://louis.uah.edu/uah-theses/695>

This Thesis is brought to you for free and open access by the UAH Electronic Theses and Dissertations at LOUIS. It has been accepted for inclusion in Theses by an authorized administrator of LOUIS.

**NUMERICAL OPTIMIZATION OF A LIQUID PROPELLANT SETTLING  
SCENARIO**

**by**

**JOSH ROJAHN**

**A THESIS**

**Submitted in partial fulfillment of the requirements  
for the degree of Master of Science in Engineering  
in  
The Department of Mechanical and Aerospace Engineering  
to  
The School of Graduate Studies  
of  
The University of Alabama in Huntsville**

**HUNTSVILLE, AL**

**2010**

In presenting this thesis in partial fulfillment of the requirements for a master's degree from The University of Alabama in Huntsville, I agree that the Library of this University shall make it freely available for inspection. I further agree that permission for extensive copying for scholarly purposes may be granted by my advisor or, in his/her absence, by the Chair of the Department or the Dean of the School of Graduate Studies. It is also understood that due recognition shall be given to me and to The University of Alabama in Huntsville in any scholarly use which may be made of any material in this thesis.

Josh Pijl      7/20/10

## THESIS APPROVAL FORM

Submitted by Josh Rojahn in partial fulfillment of the requirements for the degree of Master of Science in Engineering with an option in Aerospace Engineering and accepted on behalf of the Faculty of the School of Graduate Studies by the thesis committee.

We, the undersigned members of the Graduate Faculty of The University of Alabama in Huntsville, certify that we have advised and/or supervised the candidate on the work described in this thesis. We further certify that we have reviewed the thesis manuscript and approve it in partial fulfillment of the requirements for the degree of Master of Science in Engineering in Aerospace Engineering.

Georjin A. Rehaden 7-20-10 \_\_\_\_\_ Committee Chair

Jason T. Cassidy 7/20/10 \_\_\_\_\_

[Signature] 7-20-10 \_\_\_\_\_

Karl Frank 7/22/10 \_\_\_\_\_ Department Chair

Mark A. Fennerty 7/22/10 \_\_\_\_\_ College Dean

Chonda Kay Gaede 11/23/10 \_\_\_\_\_ Graduate Dean

## ABSTRACT

The School of Graduate Studies

The University of Alabama in Huntsville

Degree: Master of Science in Engineering in Aerospace Engineering

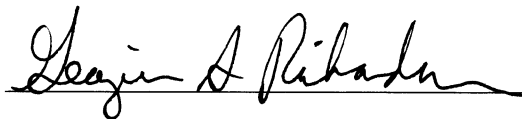
College/Department: Engineering/Mechanical and Aerospace Engineering

Name of Candidate: Josh Rojahn

Title: Numerical Optimization of a Liquid Propellant Settling Scenario

Computational fluid dynamic modeling was utilized to numerically optimize liquid propellant settling in a liquid hydrogen tank based on the Weber number. Propellant settling is the process by which thrust is provided to move the propellant to the bottom of the tank. Constant accelerations were used to simulate four different Weber numbers. Propellant settling times and the corresponding required change in velocity ( $\Delta V$ ) were calculated from the simulations for each Weber number, with the goal of optimizing the propellant settling process by minimizing  $\Delta V$ . Because the lower Weber numbers cannot be achieved in a flight-like scenario, a pulsed acceleration strategy was used to create a time averaged Weber number for comparison. The liquid propellant can be settled using the pulsing strategy, and a similar settling time can be achieved. The model was validated against a drop tower test conducted at the National Aeronautics and Space Administration's Lewis Research Center.

Committee Chair

  
\_\_\_\_\_

Department Chair

  
\_\_\_\_\_

Graduate Dean

  
\_\_\_\_\_

## **ACKNOWLEDGMENTS**

This thesis would not have been possible without a number of individuals and organizations that provided support to me during this process. My adviser, Dr. Georgia Richardson, has graciously provided technical guidance throughout this process and has been very helpful. Thank you to the other members of my committee, Professors Bardot and Cassibry.

I would like to dedicate this thesis to my family for all of their support and encouragement.

# TABLE OF CONTENTS

	Page
List of Figures .....	vii
List of Tables .....	x
List of Abbreviations .....	xi
List of Acronyms .....	xii
List of Symbols .....	xiii
Chapter	
I. Introduction.....	1
II. Analysis Tool .....	5
III. Validation.....	9
IV. Analysis Approach and Methodology .....	23
V. Constant Acceleration Analysis .....	26
VI. Pulsed Acceleration Analysis .....	51
VII. Conclusions.....	67
Appendix: AIAA Journal of Propulsion and Power Article .....	69
REFERENCES .....	78

## LIST OF FIGURES

Figure	Page
3.1 Scaled Centaur Liquid Hydrogen Test Article Geometry.....	11
3.2 Lewis Research Center Zero Gravity Facility and Test Vehicle .....	14
3.3 20,000 Cell Grid Geyser Progression .....	15
3.4 80,000 Cell Grid Geyser Impact .....	16
3.5 CFD and Test Images of Geyser Impact on Tank Top .....	18
3.6 Coarse Grid Model.....	20
3.7 CG Movement in Centaur Validation Cases.....	21
4.1 LDS Tank Geometry and Grid Methodology .....	24
5.1 Settled Propellant for $We=10$ Case.....	27
5.2 Settled Propellant for $We=100$ Case.....	28
5.3 Settled Propellant for $We=1000$ Case.....	29
5.4 Settled Propellant for 0.001g Case.....	30
5.5 CG Plots from Grid Convergence Study .....	32
5.6 CG Plots for Axisymmetric/Three-Dimensional Model Comparison .....	34
5.7 CG Plots for CFL Number Sensitivity Study .....	36



5.8	CG Plot for 0.001g Acceleration Case.....	38
5.9	CG Plot for $We = 1000$ Case .....	39
5.10	CG Plot for $We = 100$ Case .....	40
5.11	CG Plot for $We = 10$ Case .....	41
5.12	0.001g Acceleration Geysers Progression.....	43
5.13	$We = 1000$ Geysers Progression .....	44
5.14	$We = 100$ Geysers Progression .....	46
5.15	$We = 10$ Bubble Formation .....	47
5.16	Constant Acceleration Settling Time vs. Weber Number.....	48
5.17	Constant Acceleration $\Delta V$ vs. Weber Number .....	49
6.1	$We = 1000$ Geysers Progression for Constant and Pulsed Accelerations ...	56
6.2	$We = 100$ Geysers Progression for Constant and Pulsed Accelerations .....	57
6.3	$We = 10$ Geysers Progression for Constant and Pulsed Accelerations .....	58
6.4	CG Plot for $We = 1000$ Case .....	59
6.5	CG Plot for $We = 100$ Case .....	60
6.6	CG Plot for $We = 10$ Case .....	61
6.7	Settling Time vs. Weber Number .....	64

6.8	Required $\Delta V$ vs. Weber Number .....	65
A.1	LDS Tank Geometry.....	72
A.2	CG Plot for 0.001g Acceleration Case.....	74
A.3	CG Plot for $We = 1000$ Case .....	74
A.4	CG Plot for $We = 100$ Case .....	75
A.5	CG Plot for $We = 10$ Case .....	75
A.6	Settling Time vs. Weber Number .....	76
A.7	Required $\Delta V$ vs. Weber Number .....	77

## LIST OF TABLES

Table	Page
3.1 Freon-TF Fluid Properties (NASA TN-D 7168) .....	12
5.1 Settling Times for 0.001g CFL Sensitivity Study.....	37
6.1 Duty Cycle for Time Averaged Weber Numbers .....	52
6.2 Pulsed Settling Weber Numbers .....	54
6.3 Settling Time Summary for Constant and Pulsed Acceleration Cases .....	62

## LIST OF ABBREVIATIONS

Bond Number	Bo
Froude Number	Fr
Liquid Hydrogen	LH <sub>2</sub>
Liquid Oxygen	LO <sub>2</sub>
Weber Number	We

## LIST OF ACRONYMS

Center of Gravity	CG
Computational Fluid Dynamics	CFD
Computer Aided Design	CAD
Courant-Friedrich-Lewy	CFL
Lewis Research Center	LRC
Lunar Descent Stage	LDS
National Aeronautics and Space Administration	NASA
Reaction Control System	RCS
Technical Memorandum	TM
Technical Note	TN
Volume of Fluid	VOF

## LIST OF SYMBOLS

$a$	Acceleration
$ds$	Differential arc length
$f$	Liquid volume fraction
$p$	Static pressure
$R$	Tank radius
$S_{Mx}$	Source Momentum Term
$T$	Settling time
$u$	X-axis velocity component
$V$	Velocity
$\Delta V$	Change in velocity due to imposed acceleration
$x_L$	Distance from liquid-gas interface to tank bottom
$\mu$	Viscosity
$\rho$	Density
$\sigma$	Surface tension
$\partial$	Partial differential operator
$\nabla$	Gradient operator

## CHAPTER I

### INTRODUCTION

Liquid rocket engines have been employed for many different space flight vehicle applications. One popular bipropellant combination used for liquid rocket engines is Liquid Oxygen ( $\text{LO}_2$ ) and Liquid Hydrogen ( $\text{LH}_2$ ). The  $\text{LO}_2/\text{LH}_2$  bipropellant system has been used for the Space Shuttle Main Engine, Ariane 5 main and second stages, the Delta IV first stage, and the upper stages of Ares I, Saturn V, Saturn IB, Saturn I, and the Centaur stage. Additionally, the Altair vehicle will use  $\text{LO}_2/\text{LH}_2$  bipropellants for both its Lunar Descent and Ascent stages. In fact, any flight vehicle that seeks to land on the Moon, or any other planet, would require a descent stage. This thesis will examine the propellant settling process in a generic  $\text{LO}_2/\text{LH}_2$  Lunar Descent Stage (LDS). Propellant settling is the process of moving liquid to the bottom of the tank via thrust provided by an auxiliary propulsion system.

Due to the maneuvering that space flight vehicles perform and the multiple-day, microgravity cruise to Lunar orbit, it is expected that one or both of the liquid propellants are likely to be oriented unfavorably for a liquid rocket engine start. Additionally, cryogenic systems may need to perform tank venting for the purpose of tank pressure

control, which requires the liquid propellant to be oriented at the bottom of the tank. As such, it is necessary to settle the liquid to the bottom of the tank so the tank can be vented or the engine can be started without any ullage gas being ingested into the propellant feed line. To perform this settling maneuver, some sort of auxiliary propulsion system, usually a Reaction Control System, must be fired to provide a downward acceleration on the liquid propellants. This required thrust costs mass, and it will be the goal of this study to minimize that mass by minimizing the required change in velocity ( $\Delta V$ ). All else being equal, the larger the  $\Delta V$ , the larger the propellant mass required for the settling burn. The  $\Delta V$  [1] can be written as

$$\Delta V = at, \quad (1.1)$$

where  $a$  is the acceleration provided by the settling thrust and  $t$  is the time of the burn, after which the liquid propellants will be sufficiently settled for an engine start or tank vent.

This analysis will study the propellant settling process over a wide range of acceleration levels, and it is more instructive to do so by discussing the variables in terms of dimensionless parameters. The pertinent parameters to this study are the Bond and Weber numbers. The Bond number,  $Bo$ , is defined as the ratio of gravitational forces to surface tension forces, and is given by the following equation [2].

$$Bo = \frac{\rho a R^2}{\sigma} \quad (1.2)$$



$R$  is the tank radius,  $\rho$  is the density, and  $\sigma$  is the surface tension. Generally, the Bond number is only a physically meaningful quantity for capillary or microgravity flows because surface tension effects are unimportant when the Bond number is large. Tests have been conducted with Bond numbers ranging from the single digits to the hundreds. Propellant settling Bond numbers examined in this thesis will range from the single digits to the thousands. The Weber number is defined as the ratio of inertial forces to surface tension forces, and is given by the following equation, in which  $V$  is the characteristic velocity [2].

$$We = \frac{\rho V^2 R}{\sigma} \quad (1.3)$$

The velocity in the Weber number is calculated by using the following semi-empirical relation for the velocity of the flow as it impacts the tank bottom, in which  $x_L$  is the distance from the liquid-gas interface to the tank bottom [3].

$$V = \sqrt{1.8ax_L} \quad (1.4)$$

Propellant settling Weber numbers fall within the same range as the Bond number. The Froude number, by definition, is the ratio of inertial forces to gravitational forces, and is given by the following relation [2].

$$Fr = \frac{V^2}{aR} \quad (1.5)$$

In propellant settling, the Froude number is a function of tank geometry and fill level only and provides a convenient way to relate the Bond and Weber numbers.

The propellant settling problem has previously been studied in an experimental fashion at a National Aeronautics and Space Administration (NASA) facility previously known as Lewis Research Center, now part of Glenn Research Center. The Zero Gravity Facility at Glenn contains a 142 meter drop tower that has been used to conduct experiments in propellant settling and microgravity sloshing. One such propellant settling test is documented in [3], which is publicly available. This test will be used to validate the computational analysis tool which will be used in the prediction phase of this thesis. Other test reports, such as [4], which documents tests conducted in the  $We=4$  to  $We=10$  range, contain fundamental information about the various propellant settling regimes. Empirical correlations for propellant settling have been developed and are documented in these and other similar test reports.

In addition to experimentation, the propellant settling problem has been examined with other computational tools. One such tool was a two-dimensional code which was developed to study various types of tank sloshing, including propellant settling. This tool was used for at least two NASA studies on impulsive propellant settling in the late 1980's. These studies are documented in [5] and [6].

The next chapter of this thesis will explain the computational tool which was used for all of the analysis contained in this thesis. Chapter III will detail a validation study that was conducted to add confidence to the predictive calculations via a drop tower propellant settling test. Analysis methodology and model inputs for the  $LO_2/LH_2$  Lunar Descent Stage will be discussed in Chapter IV. Propellant settling analysis for the Lunar Descent Stage is contained in Chapters V and VI.

## CHAPTER II

### ANALYSIS TOOL

The propellant settling process, like other fluid flows, is governed by conservation principles. The Navier-Stokes system of partial differential equations is derived from the principles of conservation of mass, momentum, and energy. The conservation of mass equation is [7]

$$\frac{\partial \rho}{\partial t} + \nabla \cdot (\rho \vec{V}) = 0. \quad (2.1)$$

Unlike the conservation of mass equation, the conservation of momentum equation is a vector equation. For a three-dimensional problem, it yields three equations. A conservation of momentum in the x-axis is [7]

$$\frac{\partial(\rho u)}{\partial t} + \nabla \cdot (\rho \vec{V} u) = -\frac{\partial p}{\partial x} + \nabla \cdot (\mu \nabla u) + S_{Mx} . \quad (2.2)$$

Because this thesis will not address the heat transfer or thermodynamic considerations associated with this problem, the conservation of energy equation is unnecessary for solving this problem. There exists no analytical solution to the Navier-Stokes equations for the propellant settling problem, but the equations can be solved numerically in space and time over a computational domain. This process is called Computational Fluid Dynamics (CFD). First, the desired geometry is recreated, with either a Computer Aided Design (CAD) tool or with a CFD grid generator. Once the geometry model has been created, the grid model is created on the geometry model. This entails dividing the larger volume of the geometry into smaller volumes. These volumes are called cells. In the structured grid methodology of CFD-Ace+, the grid model is body fitted to the desired geometry, and the computational cells are all prisms. Once the grid model is developed, the model is prepared for simulation. There are several key components that are required in order to do this. Since this simulation is not modeling heat transfer, the fluid properties, such as density and viscosity, are given to the code as constants. Boundary and initial conditions are also required. The boundary conditions for the propellant settling problem are no-slip, adiabatic walls. The no-slip condition refers to the enforcement of zero velocity at each wall surface. The initial condition is a quiescent, curved liquid-gas interface at the 50% fill level. The CFD-Ace+ flow solver, owned by ESI-Group, is a commercially available tool that has the capabilities required to solve the propellant settling problem and is used for all analyses contained in this thesis.

The CFD-Ace+ code utilizes the finite volume approach, meaning the governing equations are numerically integrated over each computational cell, which represents a

control volume [8]. The governing equations (2.1 and 2.2) are solved at the center of each control volume or cell. The finite volume method is conservative in nature, and the Navier-Stokes equations are solved in the conservative form by CFD-Ace+. The additional requirement for solving the propellant settling problem is the ability for a CFD code to track the movement of a liquid-gas interface throughout the computational domain. The Volume of Fluid (VOF) Method is employed by CFD-Ace+ [9] to track the liquid-gas interface. The VOF Method solves for the liquid-volume fraction,  $f$ , throughout the computational domain, at every time step, via the following transport equation.

$$\frac{\partial f}{\partial t} + \nabla \cdot (\vec{V}f) = 0 \quad (2.3)$$

Cells in which  $f = 1$  are filled with liquid, while cells in which  $f = 0$  are filled with gas. Cells in which  $0 < f < 1$  contain a liquid-gas interface, and the liquid-gas interface is reconstructed with an algorithm called the Piecewise Linear Interface Construction (PLIC) method [9]. The PLIC method is the most accurate scheme that can be used in CFD-Ace+ while modeling surface tension forces. The PLIC method assumes that the liquid-gas interface is planar in each cell. Because of this, the algorithm only needs to know one point through which the interface passes and an outward pointing unit normal vector of the plane. This unit normal is parallel to the gradient of the liquid volume fraction in the cell.

Because surface tension is important for some of the propellant settling cases that will be simulated, surface tension forces must be included in the CFD model. A surface

tension force acts tangentially at the liquid-gas interface and is described by the vector equation (2.4), in which  $p$  is the static pressure,  $ds$  is differential arc length, and  $\sigma$  is the surface tension.

$$\int (\Delta p) ds = \int \sigma \vec{n} \otimes d\vec{x} \quad (2.4)$$

After the interface has been constructed, the code moves on to the next time step. The global time step is calculated based on a user input Courant-Friedrich-Lewy (CFL) condition. The CFL number is the fraction of a computational cell that can be traversed by a fluid volume in one time step. Time integration in CFD-Ace+ must be explicit when accounting for surface tension forces. In an explicit code, the spatial derivatives are discretized at the current point in time. For implicit codes, the spatial derivatives are discretized at the next time step. Since CFD-Ace+ is explicit, it is required that the CFL number be less than unity for numerical stability purposes. The default for the code for this type of problem is 0.2, and a sensitivity study will be conducted with respect to CFL number.

Once the code has solved for the velocity, pressure, and volume fraction fields and reconstructed the interface, it moves on to the next time step. The code repeats this process, marching in time, until the desired real time of the simulation has been reached. The user can then use the compatible post-processing tool, CFD-VIEW, to produce animations, still images, and extract flow variables from the solution. A special subroutine has been included in all of the calculations performed in this thesis. The subroutine records a time history of the liquid propellant center of gravity (CG), which is plotted to determine the settling time.

## CHAPTER III

### VALIDATION

While CFD-Ace+ is commercially available and has been used extensively for problems involving a liquid-gas interface, it is necessary to perform a validation study for the purpose of achieving a better understanding of the uncertainties associated with the solutions generated for this analysis. The validation study is instructive in understanding the physics that must be resolved by the CFD model. The most important information resulting from a validation study is centered around two questions. The first question is, what level of fidelity is necessary in the computational model? This question addresses order of accuracy, spatial discretization, model simplifications, and the like. For computational efficiency, it would be advantageous to perform this analysis using a two-dimensional axisymmetric grid. However, that simplification may not be valid. Additionally, numerical dissipation is a cause for concern in solving this problem. A grid that is too coarse is not likely to capture the important features of the flowfield, which may or may not be significant in calculating the settling time. The dynamics of propellant settling may be captured computationally with a model that is 1<sup>st</sup> order accurate in space and time, or they may require a higher order model.

The second question is: How close is the CFD answer compared to a physical experiment? Comparing the results from a CFD simulation to some experimentally determined result is instructive in many ways. By comparing results, a better understanding of the uncertainty in the CFD simulation can be achieved.

A drop tower test was conducted at a NASA facility called Lewis Research Center (LRC), and the 1973 test report is available to the public [3]. A scaled Centaur LH<sub>2</sub> tank was used for the test, noted as Test 2 in the test report. The tank was filled to 20% with Freon-TF, a liquid obtained from E.I. Dupont de Nemours and Co., and mounted into a test vehicle equipped with a high speed camera that captured images of the test liquid throughout the duration of the test. The test report does not explicitly state what the ullage gas is for the experiment. Since the ullage gas has no effect on the dynamic behavior of the tanked liquid, it is assumed that the ullage gas is air at room temperature. A center plane cut of the test tank geometry, with the grid model superimposed, is shown in Figure 3.1. The tank has a 7 cm radius with  $1/\sqrt{2}$  ellipsoidal domes. The Freon-TF begins the test in the top of the tank shown below, and it is desired to reorient the fluid to the tank bottom.



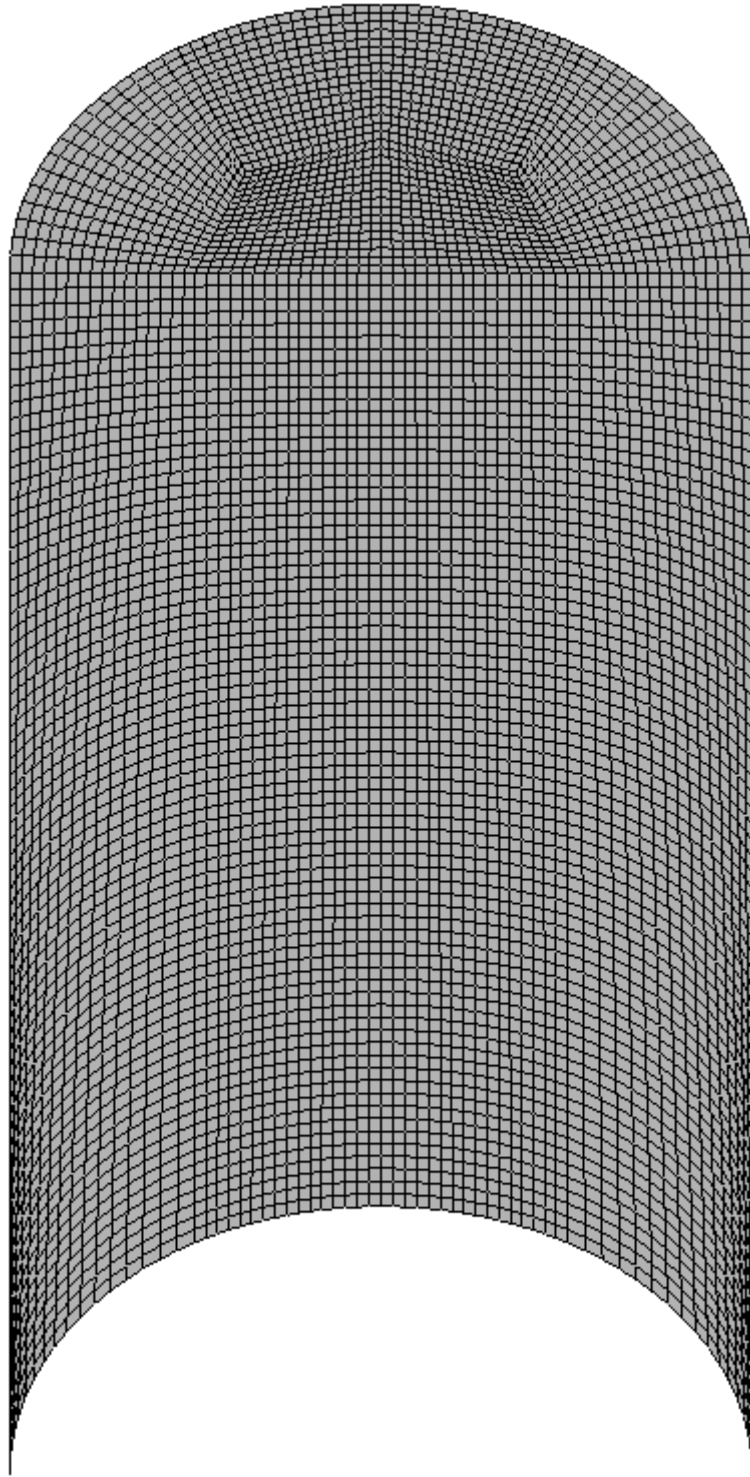


Figure 3.1: Scaled Centaur Liquid Hydrogen Test Article Geometry

The fluid properties of Freon-TF are listed in Table 3.1, and a contact angle of approximately zero degrees was observed for the liquid. The contact angle is the angle formed by the liquid when it comes into contact with the wall surface. The contact angle is important because it plays a role in the dynamics of the propellant settling process.

Table 3.1: Freon-TF Fluid Properties [3]

Density	Viscosity	Surface Tension
1580 kg/m <sup>3</sup>	0.0007 kg/(m*s)	0.0186 N/m

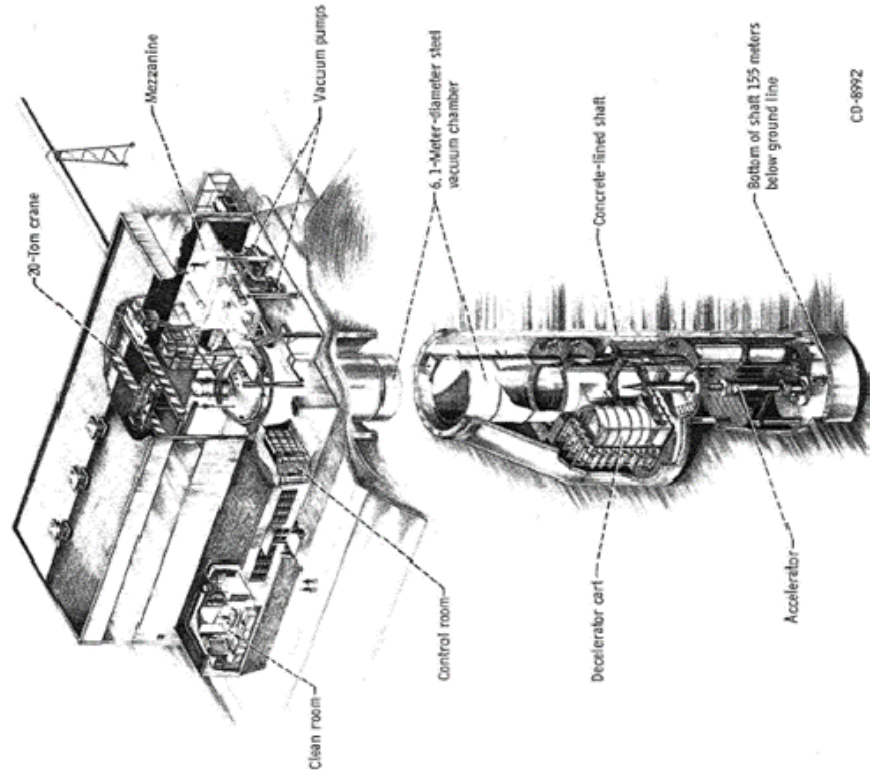
The LRC Zero Gravity Facility contains a steel vacuum chamber 142 meters deep, which allows for a free fall time of approximately 5 seconds. The test was conducted in this drop tower, which was evacuated to a pressure of 13.3 Pa. Atmospheric pressure this low creates aerodynamic drag that is on the order of  $10^{-5}$  g, three orders of magnitude below the settling acceleration delivered by the cold gas thruster system. Images of the experimental vehicle and test facility are shown in Figure 3.2.

The test vehicle is dropped down the drop tower. Simultaneously, the cold gas thruster system delivers the thrust required to simulate a Bond number of 15 in the tank. Once the liquid has had time to achieve its equilibrium position for the initial Bond number, the thruster system delivers a downward acceleration of  $0.48 \text{ m/s}^2$ , which remains constant throughout the test. This acceleration corresponds to a Bond number of 200 and a Weber number of approximately 1100. Images of the fluid dynamics inside the test are captured by the high speed camera. Once the settling thrust is activated, the liquid advances more quickly toward the bottom of the tank. The liquid impacts the

bottom of the tank and forms a geyser. The geyser progresses toward the top of the tank and impacts the top of the tank 1.27 seconds after settling thrust initiation. The geyser impact time will be extracted from the CFD performed in this thesis and compared with the experiment. Additionally, still images from the CFD model will be compared to images taken from the high speed camera on board the test vehicle.

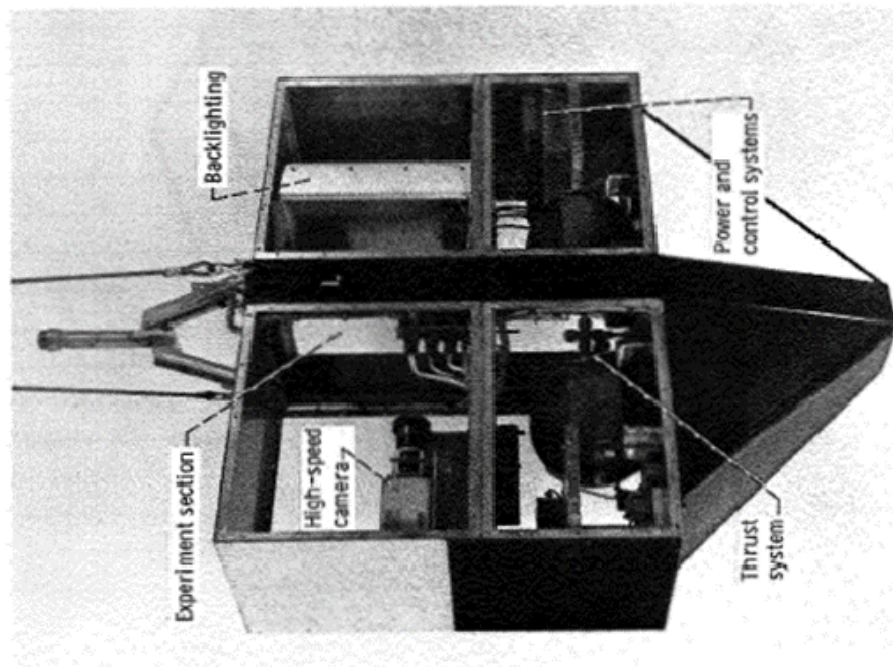
The experiment was first simulated using a coarse grid, containing 20,000 cells, for computational expediency. All simulations were performed with the 1<sup>st</sup> order accurate in space and time model, which is numerically stable. This simulation showed the initiation and progression of the geyser up the tank, but the geyser did not impact the tank top, as was demonstrated in the experiment. Additionally, this coarse grid simulation developed a volume of liquid at the top of the tank. Figure 3.3 shows the maximum progression of the geyser, but appears to show the geyser impacting the tank top. Actually, the volume of fluid from the top of the tank begins to diffuse and fall down the tank, and as the geyser reaches its maximum point in the tank, the two converge, giving the appearance of the geyser impact. For all images in this document, the pink color designates liquid, while the blue designates gas.

When the 20,000 cell CFD model did not match the test, it was determined that the model required a higher resolution. As such, the grid was refined to 80,000 cells. The validation test was again simulated, and the geyser did impact the tank top, but at a later time, 1.54 seconds, compared with the 1.27 second geyser impact time observed in the experiment. This image is shown in Figure 3.4.



CD-8992

Figure 1. - Zero Gravity Facility.



C-68-4002

Figure 2. - Experiment vehicle for low-gravity tests.

Figure 3.2: Lewis Research Center Zero Gravity Facility and Test Vehicle

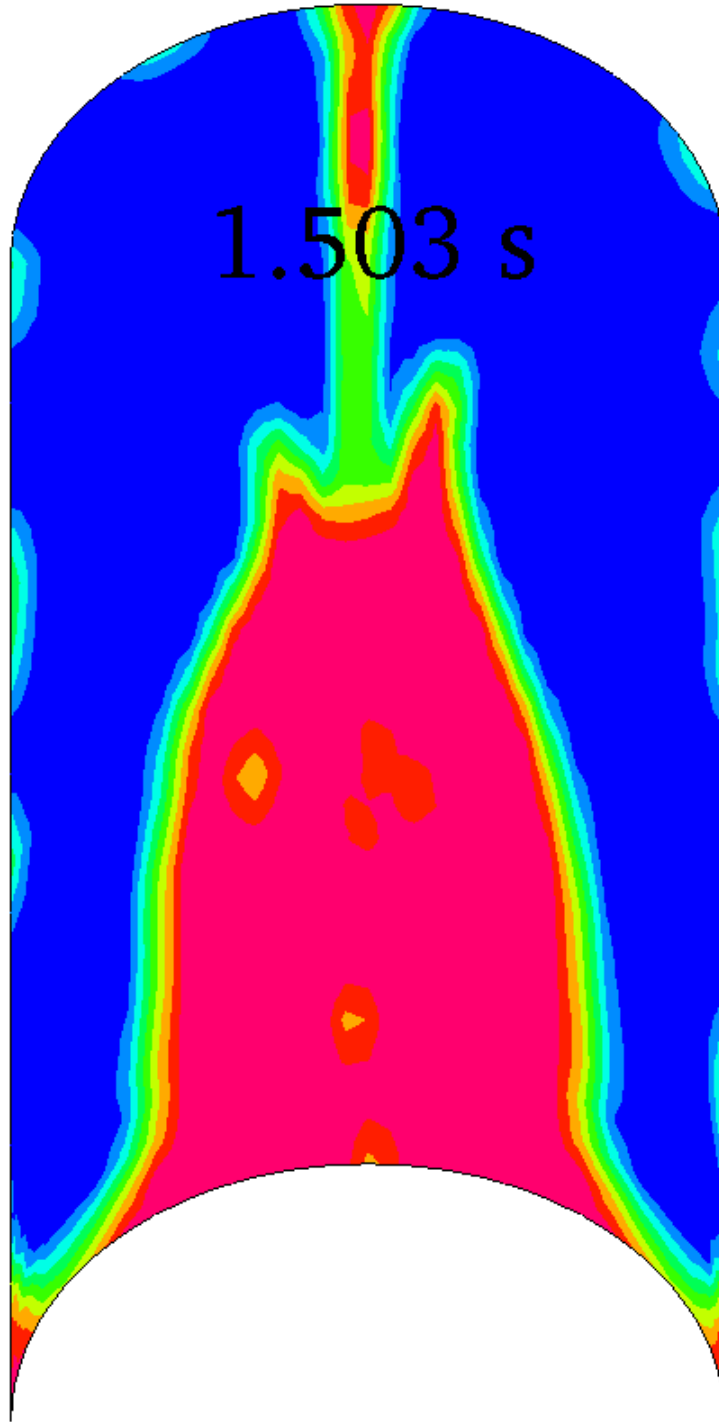


Figure 3.3: 20,000 Cell Grid Geyser Progression

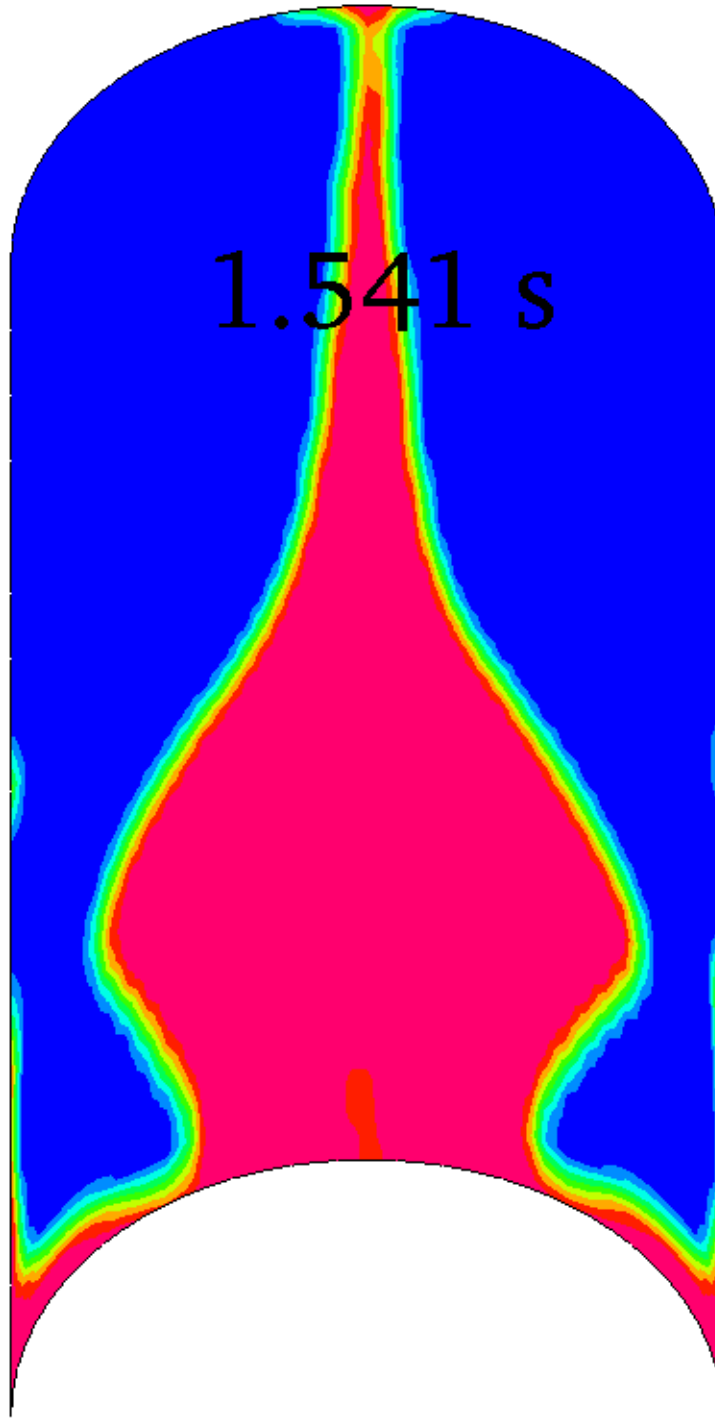


Figure 3.4: 80,000 Cell Grid Geyser Impact

Since the geyser impact time was late by 0.27 seconds, the grid was further refined to approximately 293,000 cells. Simulation of the test on this grid successfully matched the geyser impact time. After the geyser impact time was successfully matched, a sensitivity study was conducted for the contact angle of the liquid. The test reports notes an observed contact angle of zero degrees. However, without a direct measurement of the contact angle, the uncertainty in the contact angle, and its effect on the dynamics of the settling process, is unknown. Simulations were performed with contact angles of 5, 15, and 30 degrees. In the 15 and 30 degree contact angle simulations, the geyser did not impact the tank top. Results from the 5 degree contact angle simulation show a sensitivity to contact angle. It is most likely that the fluid has a near zero contact angle of no more than 5 degrees. Figure 3.5 shows the geyser impact for the experiment, as compared with the CFD models for contact angles of zero and 5 degrees.

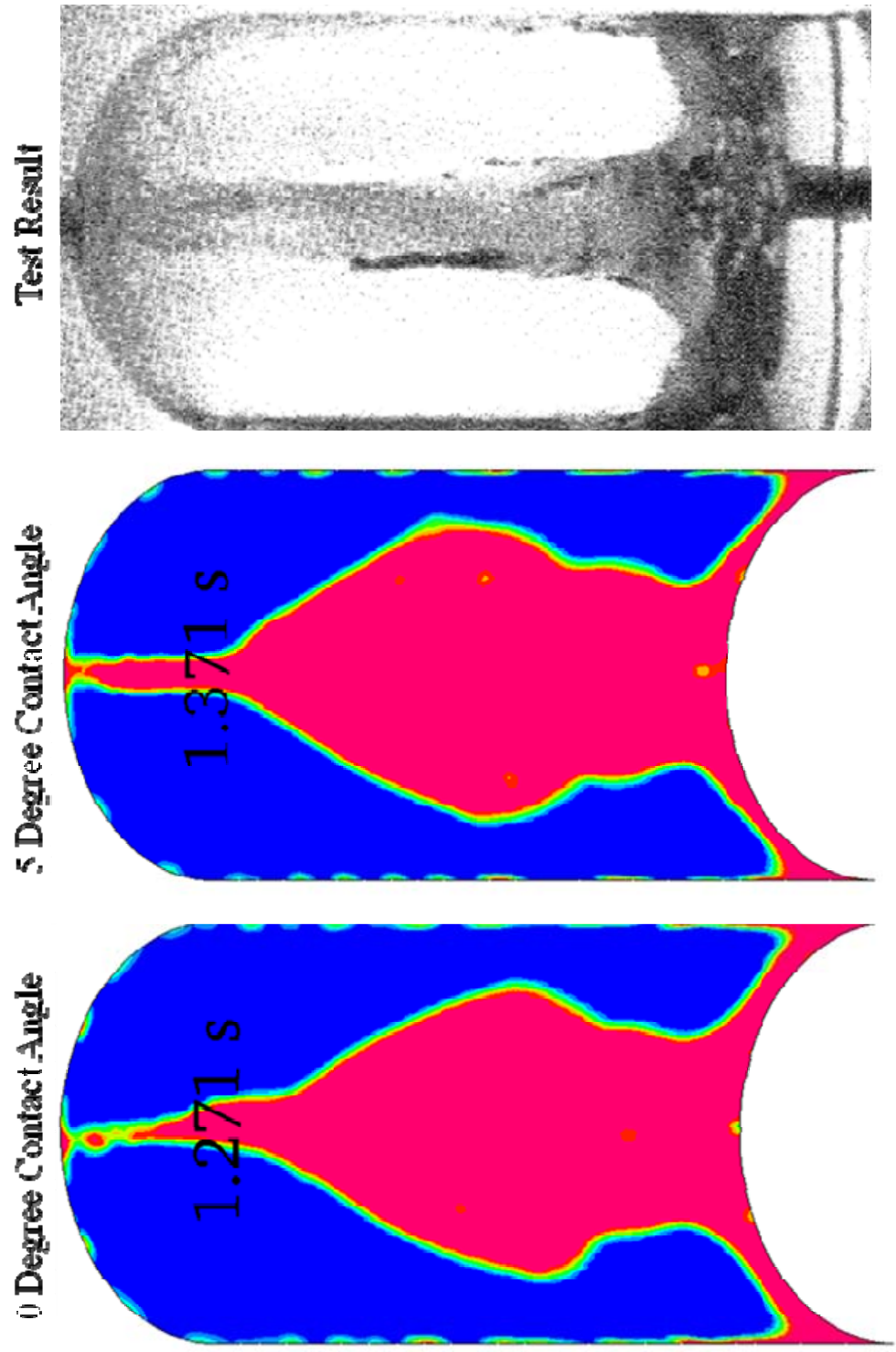


Figure 3.5: CFD and Test Images [3] of Geyser Impact on Tank Top



The still images from the CFD model show that the geyser impact time matches the test very closely. The most significant difference between the test and CFD model is the shape of the geyser. The shape is well matched at the bottom of the tank, but CFD shows a thicker geyser near the middle of the tank and a thinner geyser near the top of the tank.

For the prediction part of this thesis, propellant settling times will be calculated based on the longitudinal center of gravity (CG) movement of the tanked liquid. Because of this, it is important to study the CG movement seen in the Centaur validation simulations. This was not recorded from the experiment, so there is no test data for comparison, but it is instructive to see the difference between the fine grid, the coarse grid, and a two-dimensional axisymmetric case that was run for comparison. The axisymmetric model utilized the same grid spacing as is seen in Figure 3.1. An image of the coarse grid model is shown in Figure 3.6. Figure 3.7 shows the longitudinal CG movements from these cases, including the coarse grid containing 20,000 cells, the fine grid containing 293,000 cells with zero and 5 degree contact angle simulations, and an axisymmetric simulation using the same grid spacing as the fine three-dimensional grid.

In making an axisymmetric simplification, the dynamics of the propellant settling process are forced to occur in two dimensions. This results in a non-physical model in which the instabilities associated with the liquid-gas interface cannot be captured. The asymmetries present in the three dimensional simulations show that the three-dimensional model is capturing some of these instabilities. The axisymmetric model is not valid here, but another comparison will be made for predictive calculations.

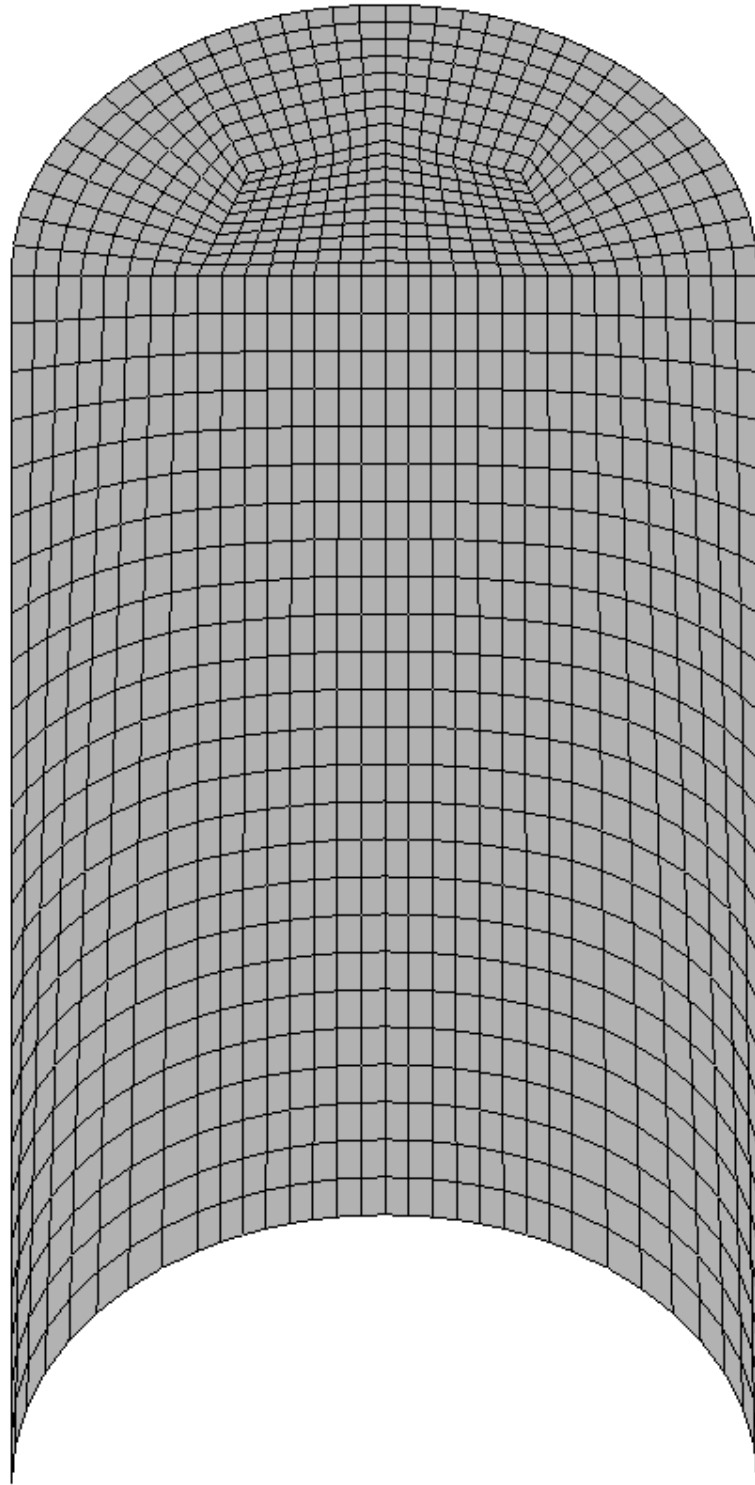


Figure 3.6: Coarse Grid Model

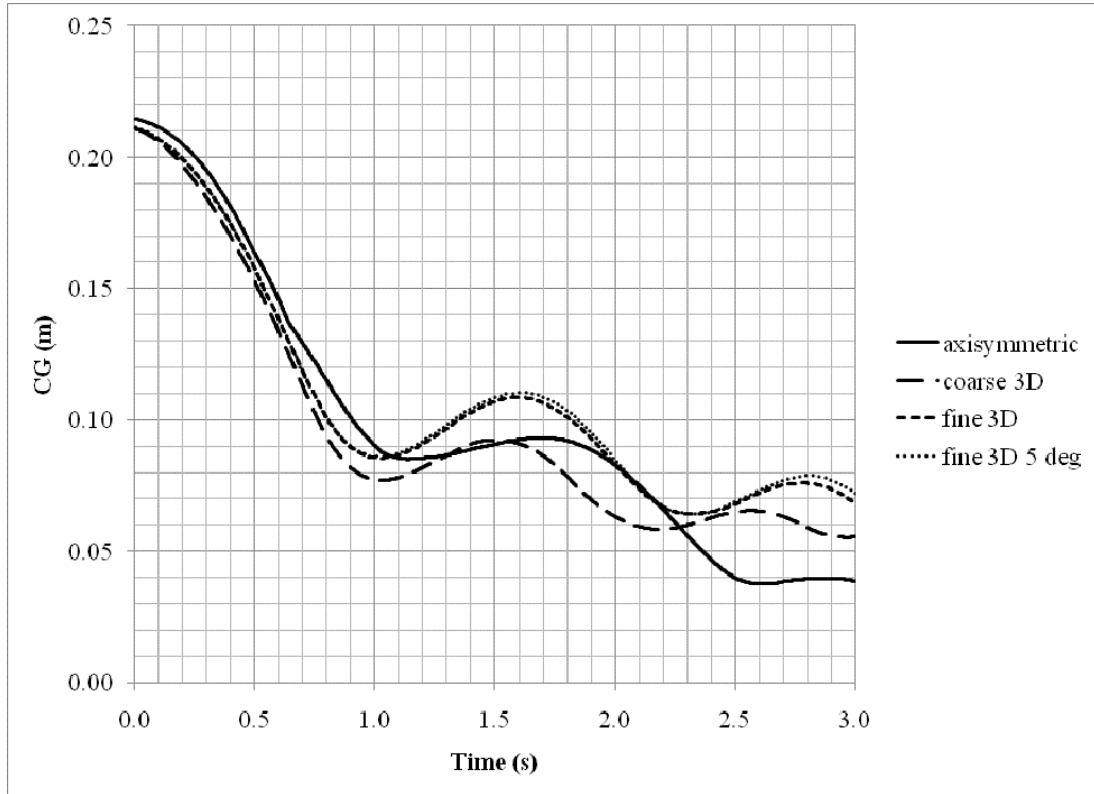


Figure 3.7: CG Movement in Centaur Validation Cases

Figure 3.7 shows little sensitivity to contact angle between zero and 5 degrees for the fine mesh. The coarse and fine grid solutions differ from each other because the geyser is more numerically diffused in the coarse grid solution. Since this thesis is focused on settling propellant sufficiently for an engine start or tank vent, it should be noted that the liquid in the centaur test tanks is not sufficiently settled at the end of the tests.

Because the contact angle between the liquid and tank wall was not measured, but observed, it is necessary to perform an uncertainty calculation associated with the parameter. After performing the sensitivity study, it was found that a 5 degree contact angle caused the geyser impact time to be later than what was seen in the experiment. As a measure of uncertainty associated with the contact angle and its importance in predictive propellant settling calculations, it is necessary to calculate the maximum L1 error caused by the contact angle of 5 degrees. This value, using the fine grid with zero contact angle as the basis, is calculated to be less than 5.7%. This uncertainty is within the margin that would need to be applied to any predictive calculations.

A validation study has been conducted using the CFD-Ace+ tool. It was found that the code is capable of capturing the propellant settling geyser impact time when enough cells are used in the CFD model. Because the prediction phase of this thesis will examine the CG movement of the bulk liquid in a tank during the propellant settling process, the difference in the geyser shape will have to be accounted for by applying a margin. A grid independent settling time will be sought for the predictive calculations.

## CHAPTER IV

### ANALYSIS APPROACH AND METHODOLOGY

The goal of this thesis is to minimize the  $\Delta V$  required for settling a liquid propellant in a flight-like tank. Due to the variability in possible designs for a LDS, there are many possible tank geometries. However, analysis will be conducted based on the Weber number, a dimensionless parameter that contains information about the tank geometry, propellant fill level, fluid properties, and vehicle acceleration. The Weber number was defined in equation (1.3). The tank analyzed in this thesis will be a 28.32 m<sup>3</sup> (1000 ft<sup>3</sup>) cylindrical LH<sub>2</sub> tank with 1/ $\sqrt{2}$  ellipsoidal, convex end caps. The tank radius was chosen to be 1.52 m (5 ft), requiring a tank barrel length of 2.44 m (8 ft). The tank geometry for this LDS is shown below in Figure 4.1 along with a cross section of the baseline structured grid used for the calculations.

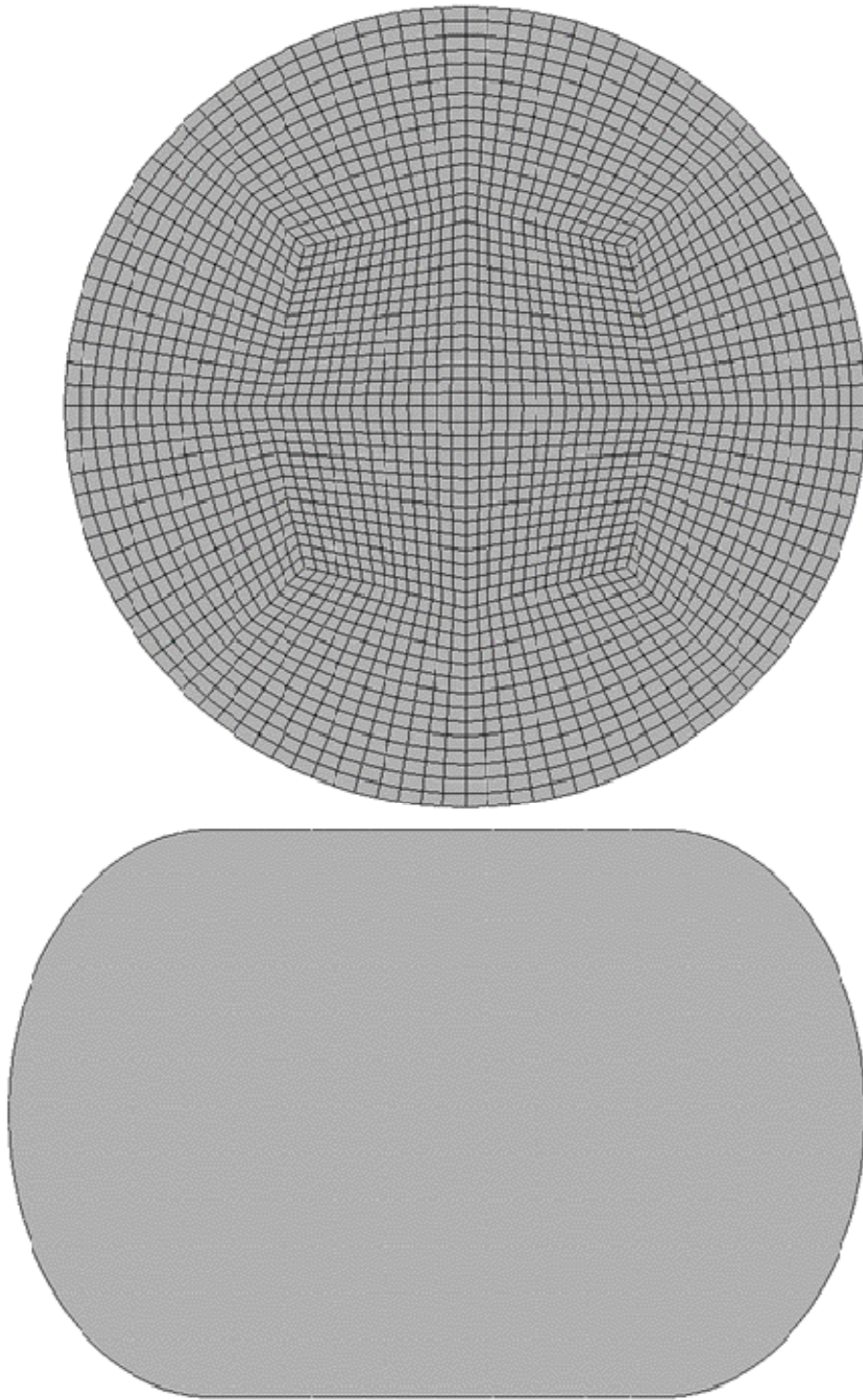


Figure 4.1: LDS Tank Geometry (bottom) and Grid Methodology (top)

This LDS propellant system will utilize cryogenic LO<sub>2</sub> and LH<sub>2</sub> bipropellants. The justification for studying the LH<sub>2</sub> only is that for any given flight-like configuration, since both propellants will experience the same acceleration, the Bond and Weber numbers for the LO<sub>2</sub> will be greater than the Bond and Weber numbers for the LH<sub>2</sub>. Put another way, if the LH<sub>2</sub> is settled, the LO<sub>2</sub> will be settled as well.

Due to the long duration of microgravity coast between Low Earth Orbit and the Moon, the worst case initial condition will be imposed for the LH<sub>2</sub> propellant. That is, all of the propellant will be located in the top of the tank with a quiescent surface. The tank will be half full with LH<sub>2</sub> for this analysis. The ullage will be helium, a common pressurant gas used for liquid propellant tanks.

Since it is the goal of this analysis to minimize the  $\Delta V$  based on the Weber number, a constant acceleration settling analysis will first be done at four different acceleration levels. Simulations of the settling process will be performed at Weber numbers of 10, 100, and 1000. An additional simulation will be performed with an acceleration of 0.001g, which is the order of magnitude of acceleration that a typical RCS could deliver. Since it is not possible for an RCS to throttle down by orders of magnitude, an additional analysis will be conducted in which the propellant will be accelerated in a pulsing fashion. This pulsing will create a time averaged Weber number that will come very close to matching the desired Weber number from the constant acceleration analysis.

## CHAPTER V

### CONSTANT ACCELERATION ANALYSIS

Prior to conducting an in-depth analysis, a condition must be defined at which the propellant is deemed to be sufficiently settled. Since the longitudinal CG of the liquid propellant will be tracked throughout the simulation, the propellant will be deemed to be settled when the value of the CG crosses some threshold value. Each simulation will be performed with the goal of determining one threshold value that is adequate for all four cases. The four cases are 0.001g acceleration and Weber numbers of 10; 100; and 1,000. After post-processing each simulation, it was found that when the longitudinal CG crossed the threshold value of 0.6 m (~2 ft) above the bottom of the barrel section, the liquid propellant was sufficiently oriented toward the bottom of the tank. The limiting case was the 0.001g acceleration case, in which vapor bubbles were entrained in the liquid. These bubbles must be clear of the tank outlet prior to engine start. Figures 5.1 through 5.4 show center plane cut images of the liquid volume fraction for each acceleration case at the settling time. The pink color represents liquid propellant, and the blue represents the ullage gas.



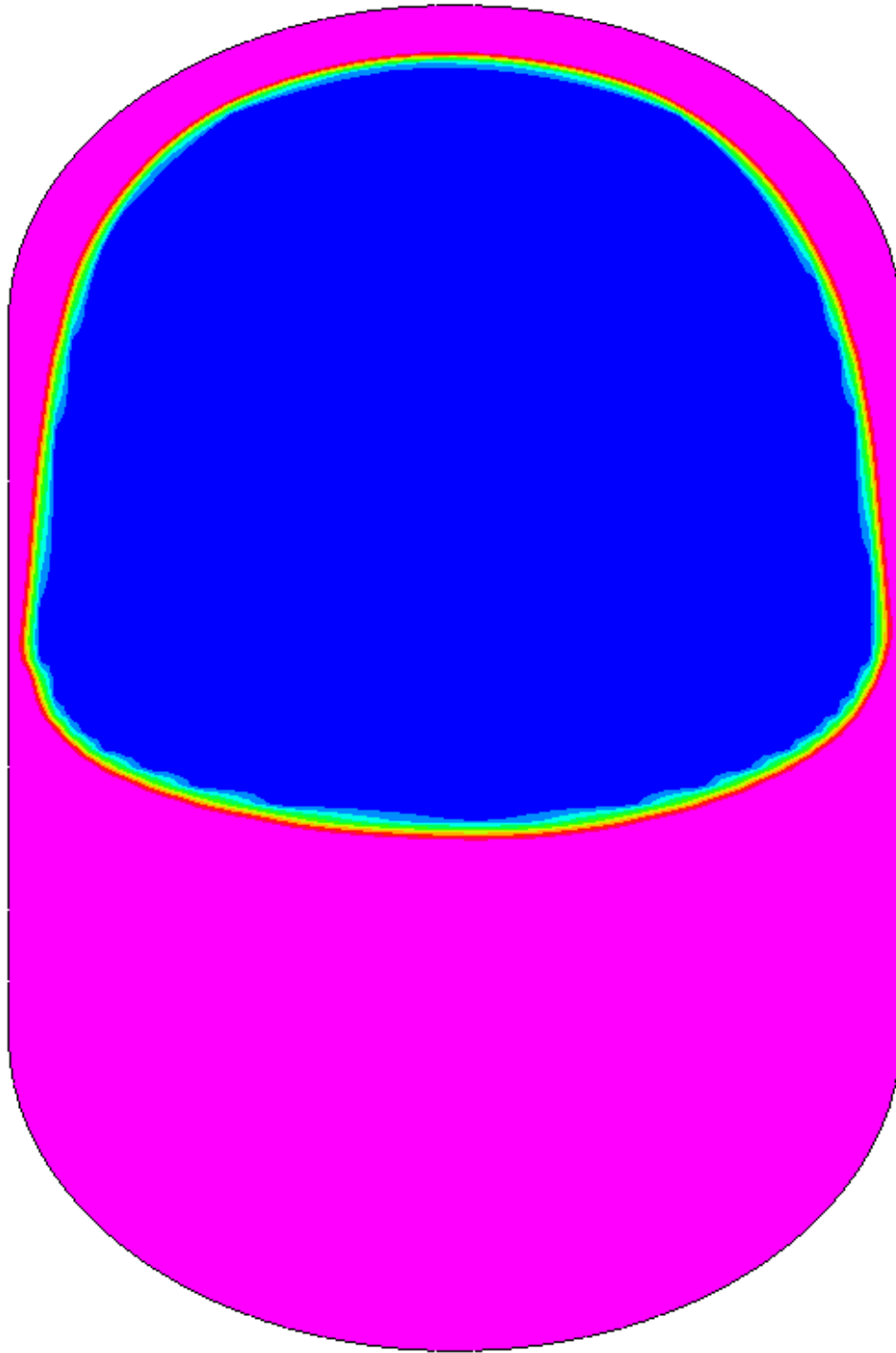


Figure 5.1: Settled Propellant for  $We=10$  Case

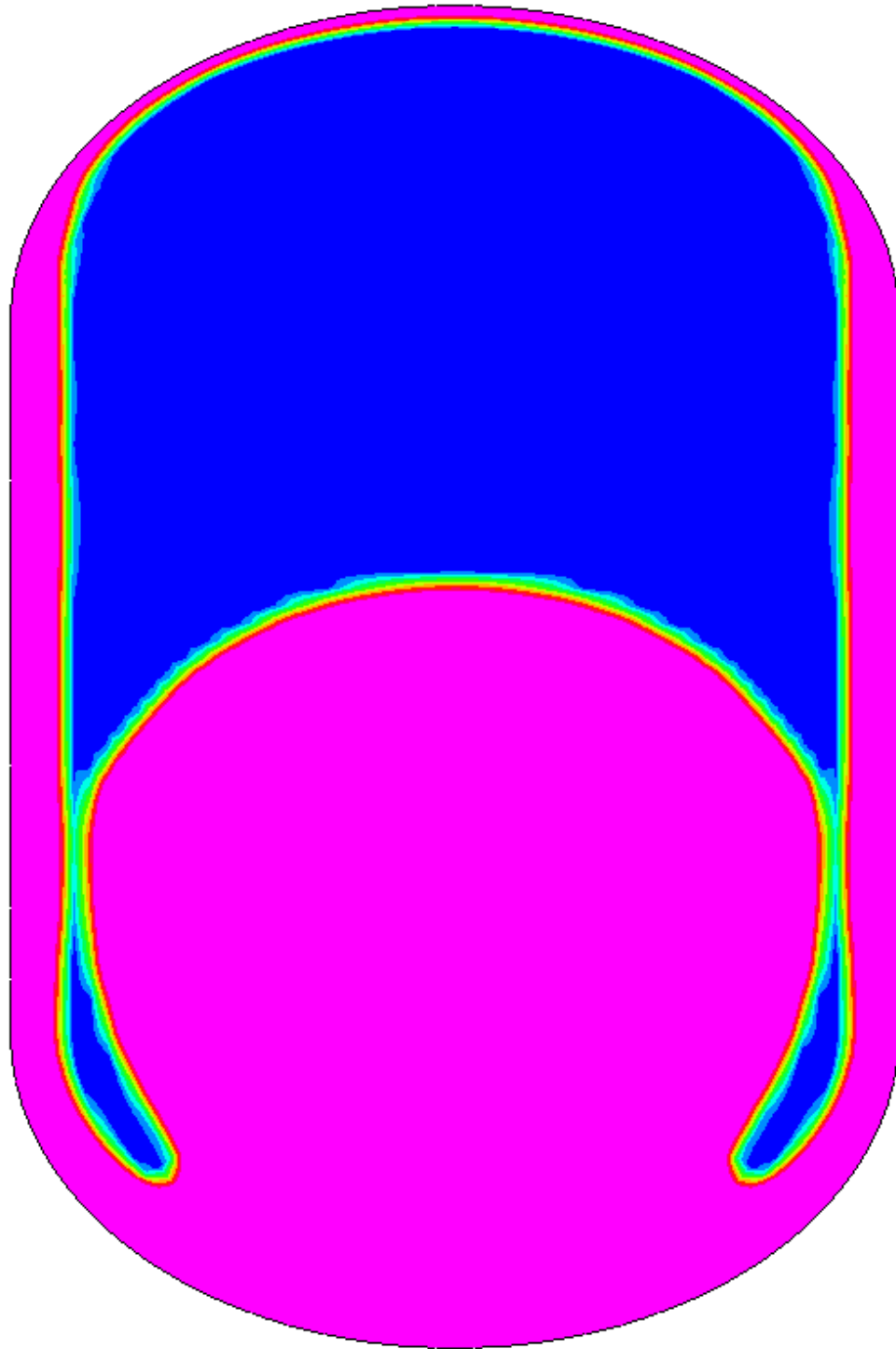


Figure 5.2: Settled Propellant for  $We=100$  Case



Figure 5.3: Settled Propellant for  $We=1000$  Case

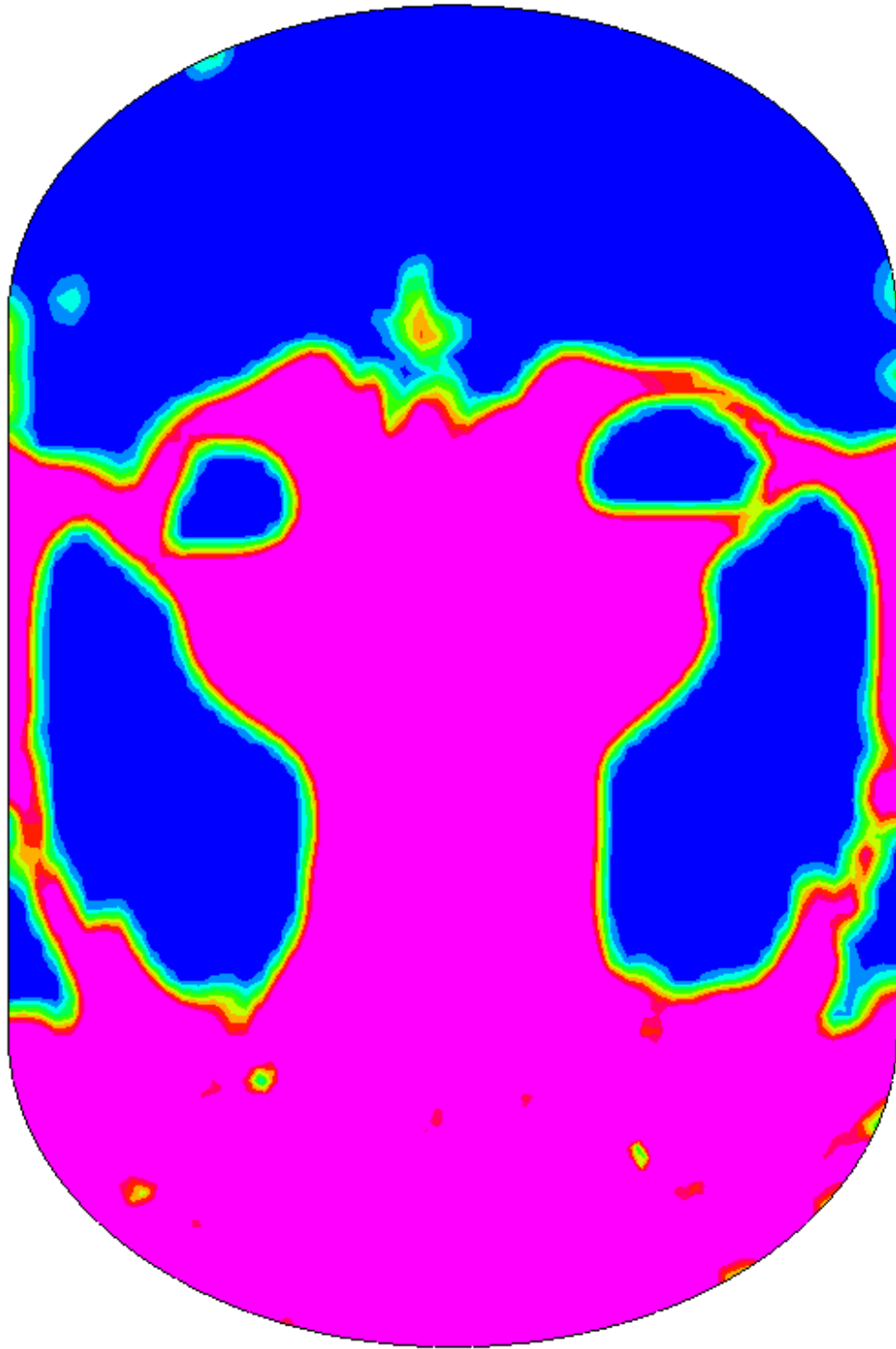


Figure 5.4: Settled Propellant for 0.001g Case

In order to have confidence that the liquid propellant was sufficiently settled at the chosen threshold value, it was necessary to ensure that the solution was grid converged. The baseline grid contained approximately 182,000 cells, and it was refined to 640,000 cells to check for grid convergence. Simulations were performed for the 0.001g acceleration case, which was the only case suitable for simulation on the 640,000 cell grid due to the required computation time. Figure 5.5 shows the longitudinal CG plots for both grids. The settling time for the 182,000 cell grid was 114 seconds, and the settling time for the 640,000 cell grid was 112 seconds, indicating a grid converged settling time. After 120 seconds, which is the limit shown on the graph, the propellant CG asymptotically approaches the value it would be for a half full tank on the ground. The solid line on Figure 5.5 shows the settled CG value.

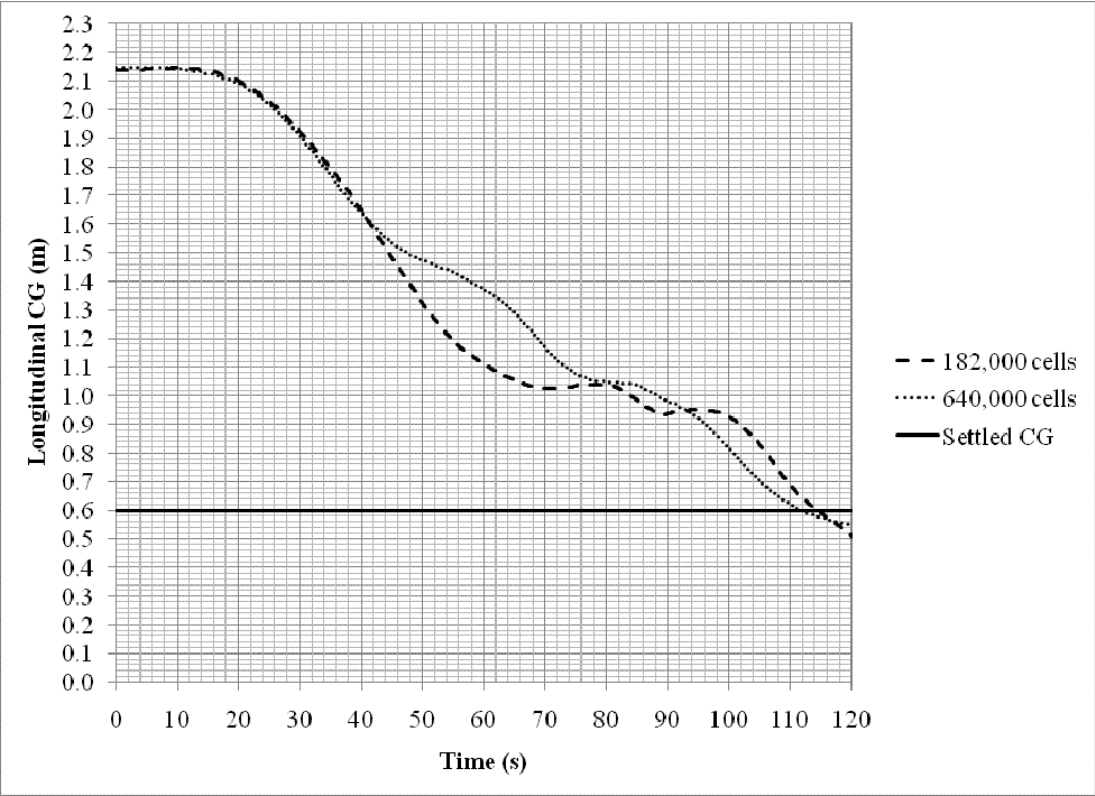


Figure 5.5: CG Plots from Grid Convergence Study

Now that propellant settling has been defined and a grid converged three-dimensional solution exists, the required level of fidelity of the model will be studied. Due to the large simulation time that is required, especially for the smaller Weber numbers, it would be advantageous to model the propellant settling problem for this LDS with an axisymmetric model. Simulation times would decrease drastically, and future studies could be performed with an axisymmetric model. However, the level of fidelity of the model would be lower, and the axisymmetric grid solution must also be grid independent. It may be the case that the propellant settling dynamics are three-dimensional, and there is no shortcut that can be taken to model this problem axisymmetrically. The test for this will be comparing axisymmetric simulations with the three-dimensional simulations for the 0.001g case. For this study, the requirement for axisymmetric modeling is that the solution must achieve grid independence while calculating a settling time within  $\pm 10$  percent of the grid independent three-dimensional value. Figure 5.6 shows the longitudinal CG plots from the axisymmetric simulations when compared to the three-dimensional simulations. The plots indicate that the axisymmetric model cannot produce a grid independent solution. The grid spacing in the 5,600 cell axisymmetric grid is identical to the grid spacing in the 640,000 cell three-dimensional grid. Similar to the validation experiment, the axisymmetric model is non-physical because of the requirement that momentum be conserved in two dimensions. Instabilities are not captured with the axisymmetric model, and it is required that all predictive calculations be performed in three dimensions.

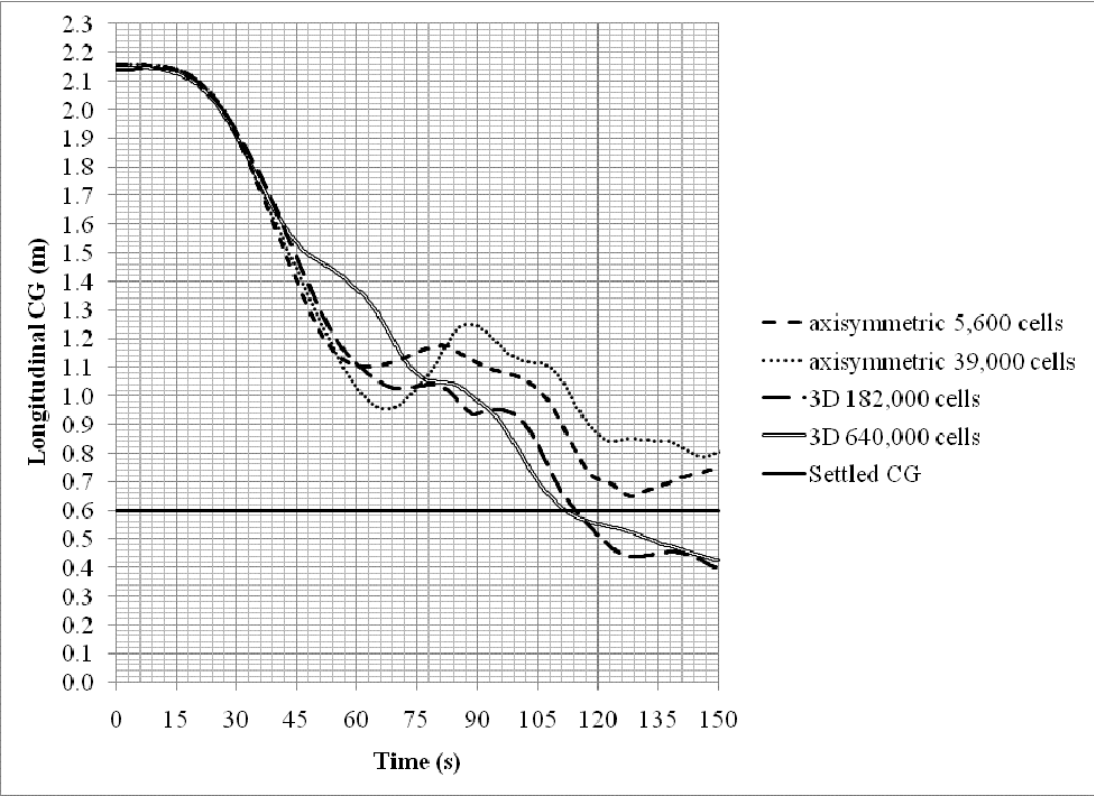


Figure 5.6: CG Plots for Axisymmetric/Three-Dimensional Model Comparison



After significant refinement from approximately 5,600 cells to 39,000 cells, the axisymmetric solutions were still grid dependent, and the finer grids were producing solutions that diverged significantly from the three-dimensional grid independent solution. Additionally, the axisymmetric grid solutions never crossed the required CG threshold for adequate propellant settling. It was concluded that the three-dimensional model is necessary and that the 182,000 cell grid was sufficient for producing grid independent settling times.

CFD simulations can be sensitive to more than just grid resolution. They can also be sensitive to time step, or in this case, the user chosen CFL number. A CFL number of 0.2 was used for all of the previous calculations, and it is good practice to ensure that the CFL number is not so high or low that it causes numerical stability issues. Also, a CFL number that is too high will not resolve all of the dynamics. Simulations were run with 0.001g constant acceleration on the 182,000 cell three-dimensional grid with CFL numbers of 0.1 and 0.3 to compare to the baseline simulation. The longitudinal CG plots are shown in Figure 5.7.

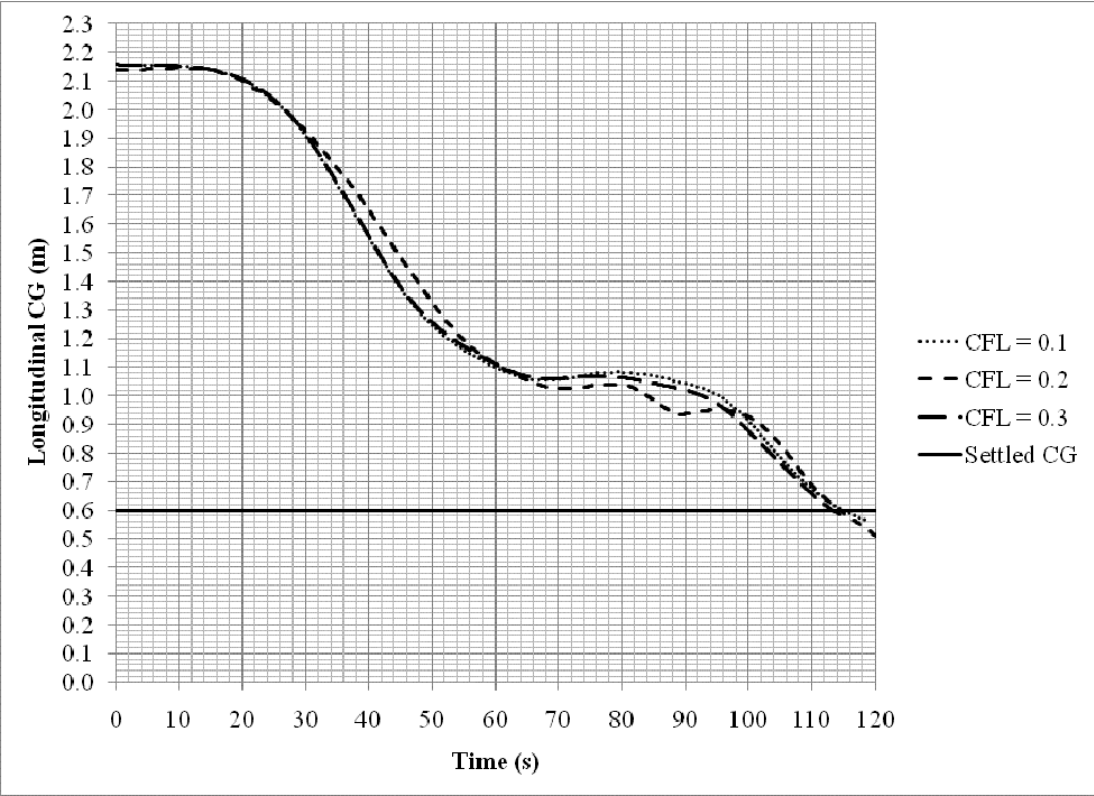


Figure 5.7: CG Plots for CFL Number Sensitivity Study

Figure 5.7 shows the sensitivity of the CG movement to CFL number for a stable, acceptable range of CFL. Table 5.1 gives the settling times for the 0.001g cases with variable CFL number. It is concluded that the settling time is independent of CFL number.

Table 5.1: Settling Times for 0.001g CFL Sensitivity Study

CFL Number	Settling Time (s)
0.1	115
0.2	114
0.3	113

Now that all of the necessary solution verification activities have been performed, the analysis results will be presented. Longitudinal CG plots for each of the four acceleration cases are shown in Figures 5.8 through 5.11.

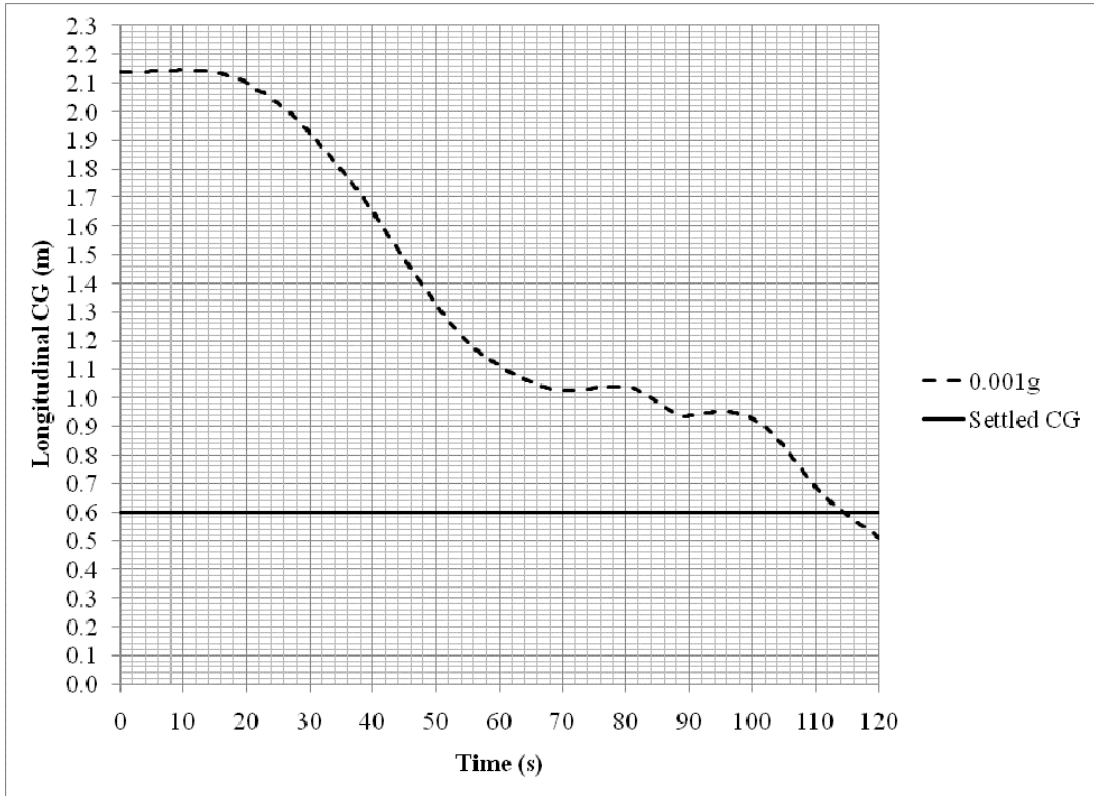


Figure 5.8: CG Plot for 0.001g Acceleration Case

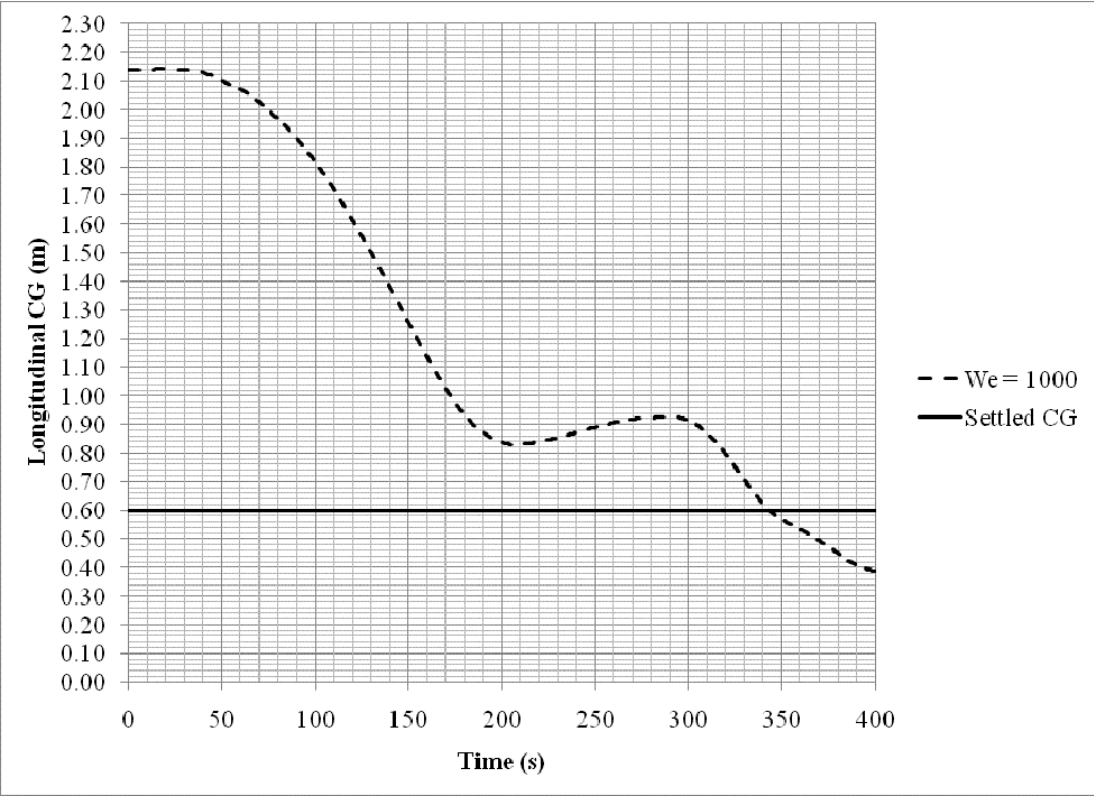


Figure 5.9: CG Plot for We = 1000 Case

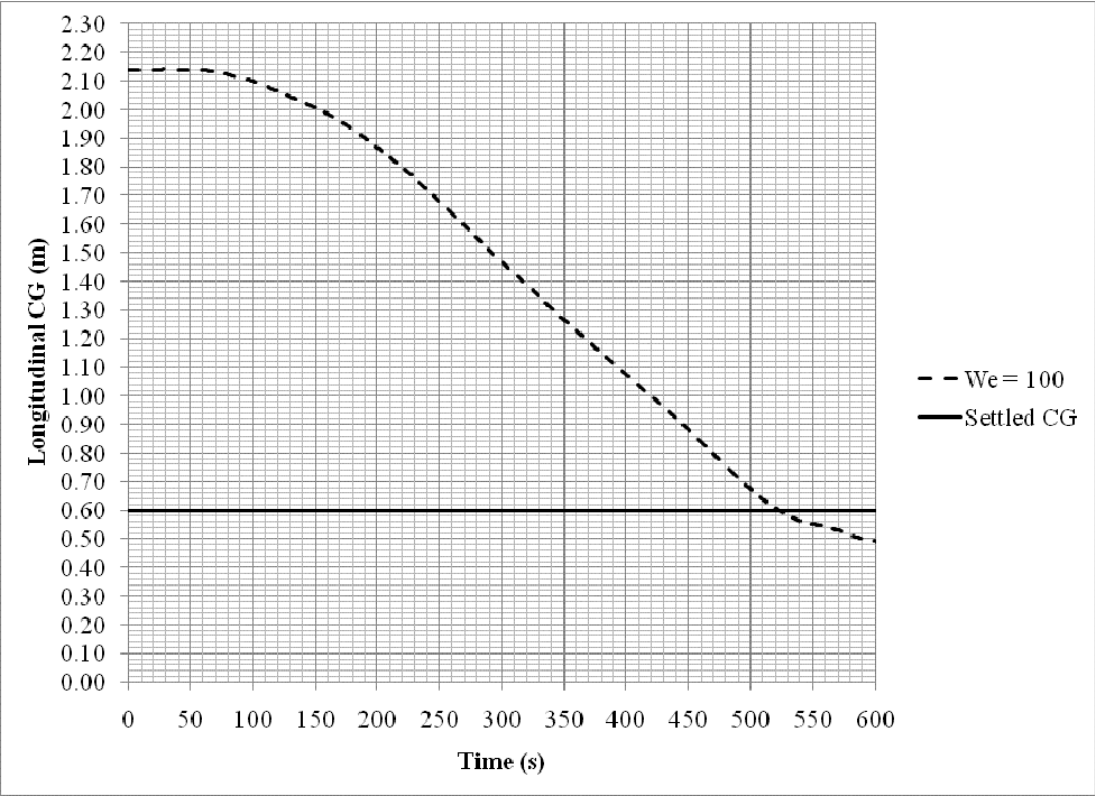


Figure 5.10: CG Plot for We = 100 Case

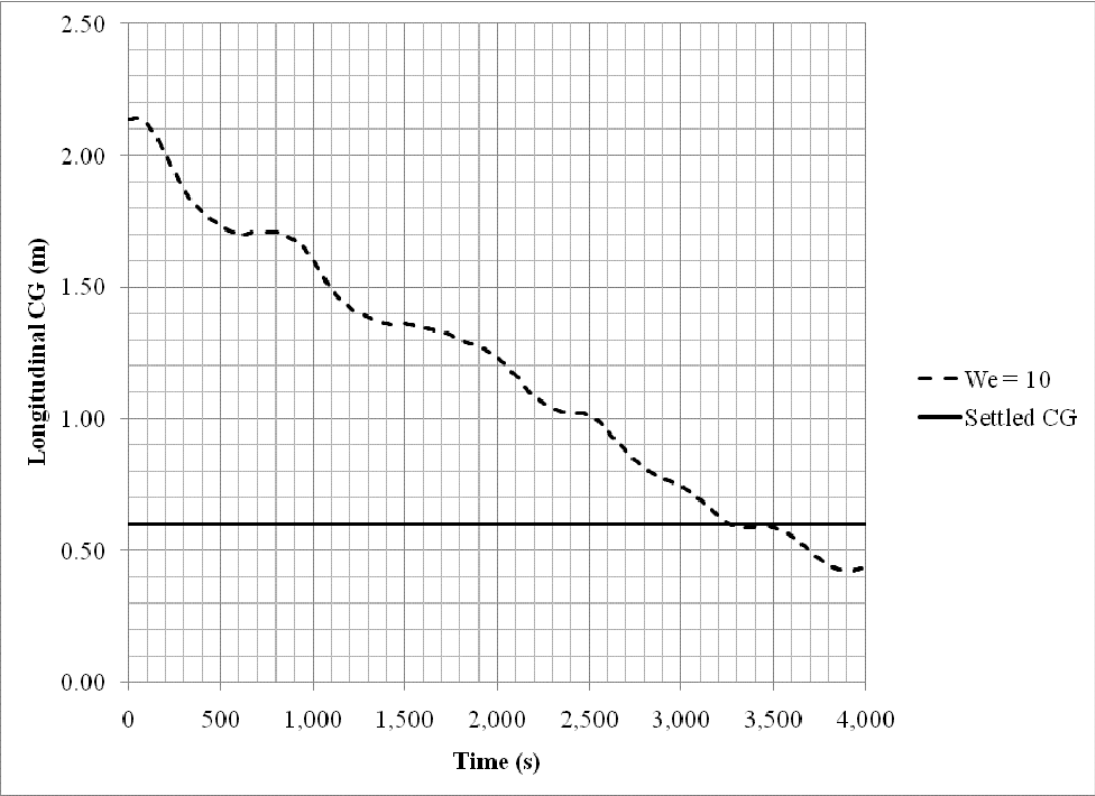


Figure 5.11: CG Plot for We = 10 Case

Figures 5.8 through 5.11 show the longitudinal CG plots for the four acceleration values studied in this thesis. The dynamics at each acceleration level differ because they fall into different regimes. These dynamics will be discussed prior to the determination of settling times. It is clear that geysers form in the tank for the 0.001g and  $We = 1000$  cases because of the inertia of the fluid as it converges in the tank's aft dome. Images of the maximum progression of the geysers are given in Figure 5.12 for the 0.001g case and in Figure 5.13 for the  $We = 1000$  case. Neither geyser impacts the tank's forward dome. In the 0.001g acceleration case, the geyser impacts some of the tanked liquid, which halts its progression. In the  $We = 1000$  case, the geyser progresses up the tank, but its inertia is overcome by gravity in the middle of the barrel section. Neither of the CG plots for these cases show a significant rebounding of the CG due to the geyser. This is due to the fact that the liquid that is not part of the geyser is still progressing down the tank, creating less pronounced curvature in the CG plots.





Figure 5.12: 0.001g Acceleration Geyser Progression

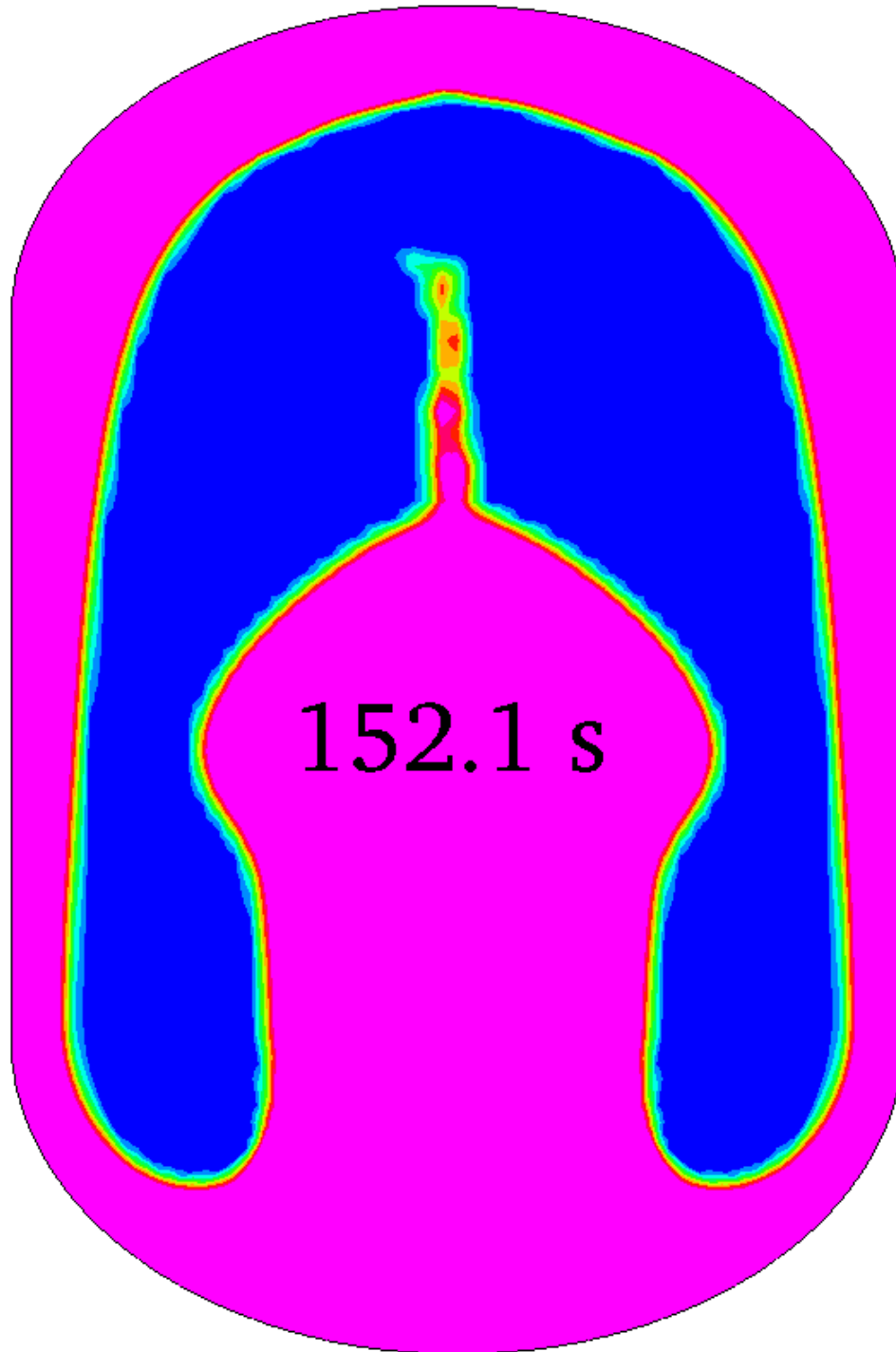


Figure 5.13:  $We = 1000$  Geyser Progression

It is not expected that the  $We = 100$  case will develop a geyser that traverses through much of the tank, given the results from the higher acceleration simulations. Figure 5.14 shows an image of the geyser's progression. A geyser forms in the tank and progresses to the middle of the barrel section, where its upward progression stops. Throughout the simulation, the geyser grows in width and eventually diffuses into the bulk liquid.

Surface tension forces are only significant for the  $We = 10$  case. An oscillatory bubble, rather than a geyser, is formed in the liquid that unsteadily changes shape and orientation. This bubble moves around the tank, and over time, toward the top of the tank. Its oscillations in time can be seen in the CG plot in Figure 5.11. Figure 5.15 shows an image of the bubble after it has formed.

Now that the dynamics of the propellant settling process have been explained for the four cases, the settling times will be plotted against the Weber number on a logarithmic scale. Figure 5.16 shows the trend of decreasing settling time with increasing Weber number. The discrete data points have been connected for clarity.

For the LDS being optimized in this thesis, the parameter of concern is  $\Delta V$ . Minimizing  $\Delta V$ , as previously noted, minimizes the amount of propellant burned during the settling process. The  $\Delta V$  is given by Equation 1.1 and is plotted in Figure 5.17 against Weber number on a logarithmic scale.

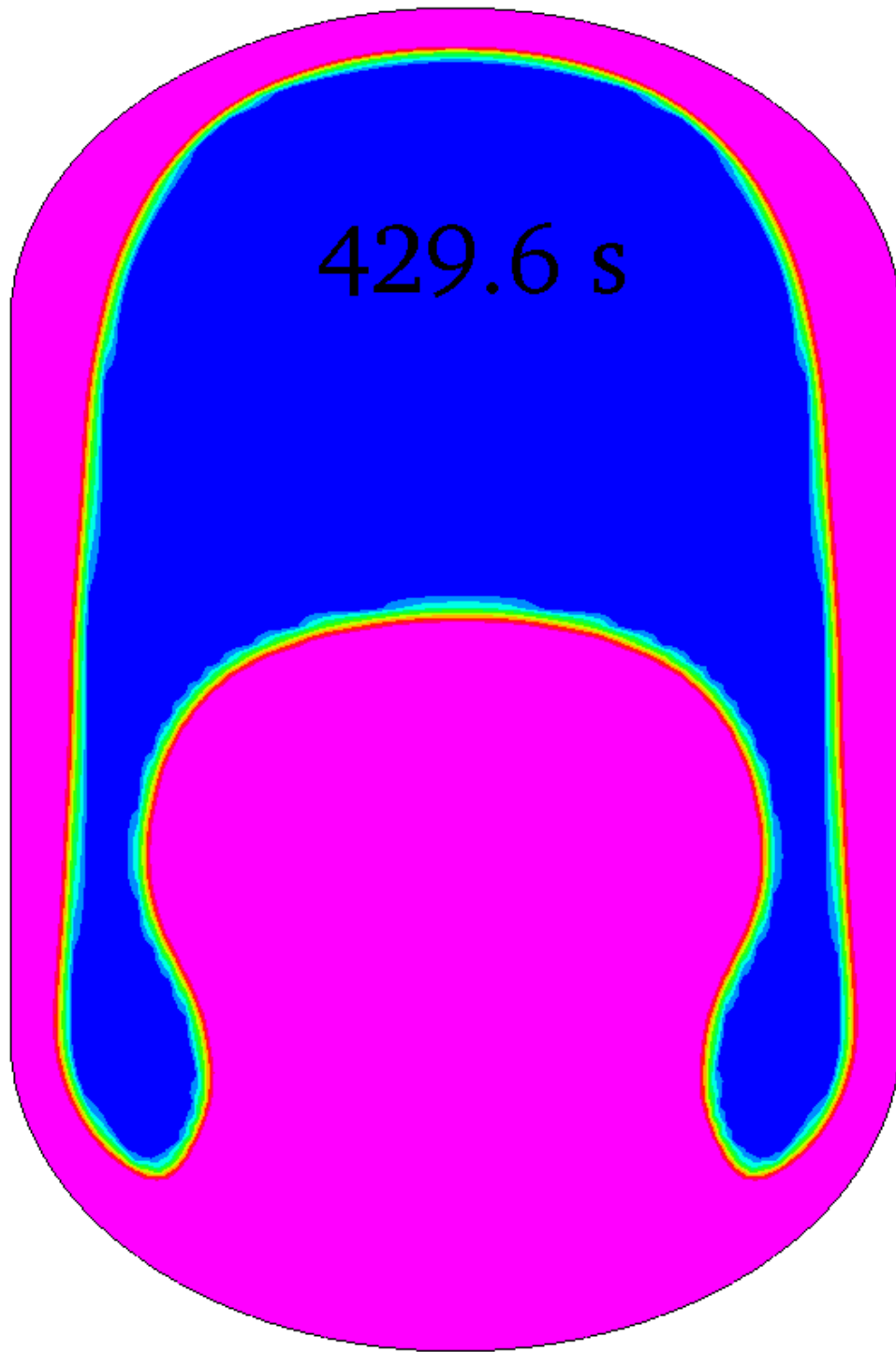


Figure 5.14:  $We = 100$  Geyser Progression

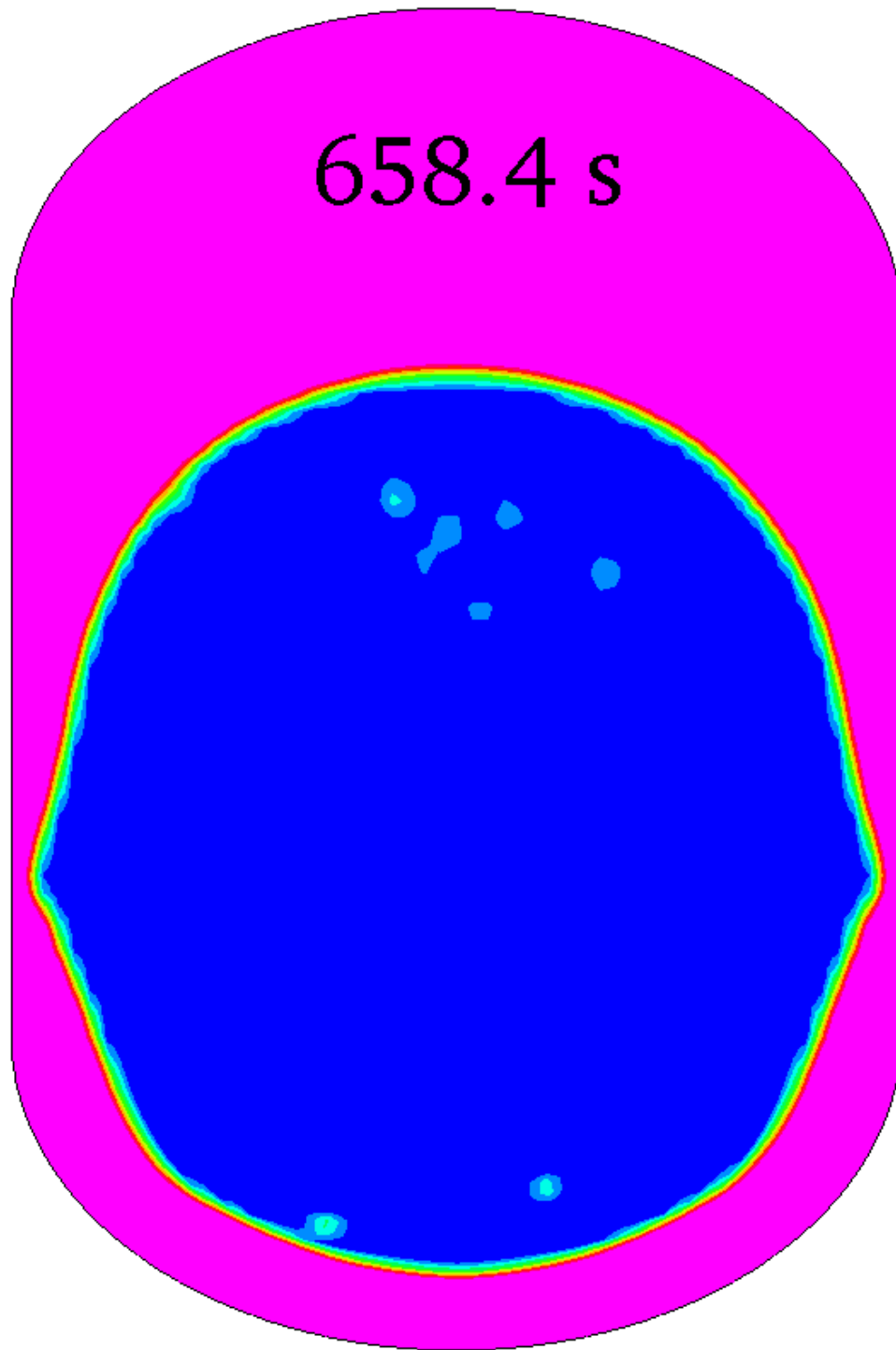


Figure 5.15:  $We = 10$  Bubble Formation

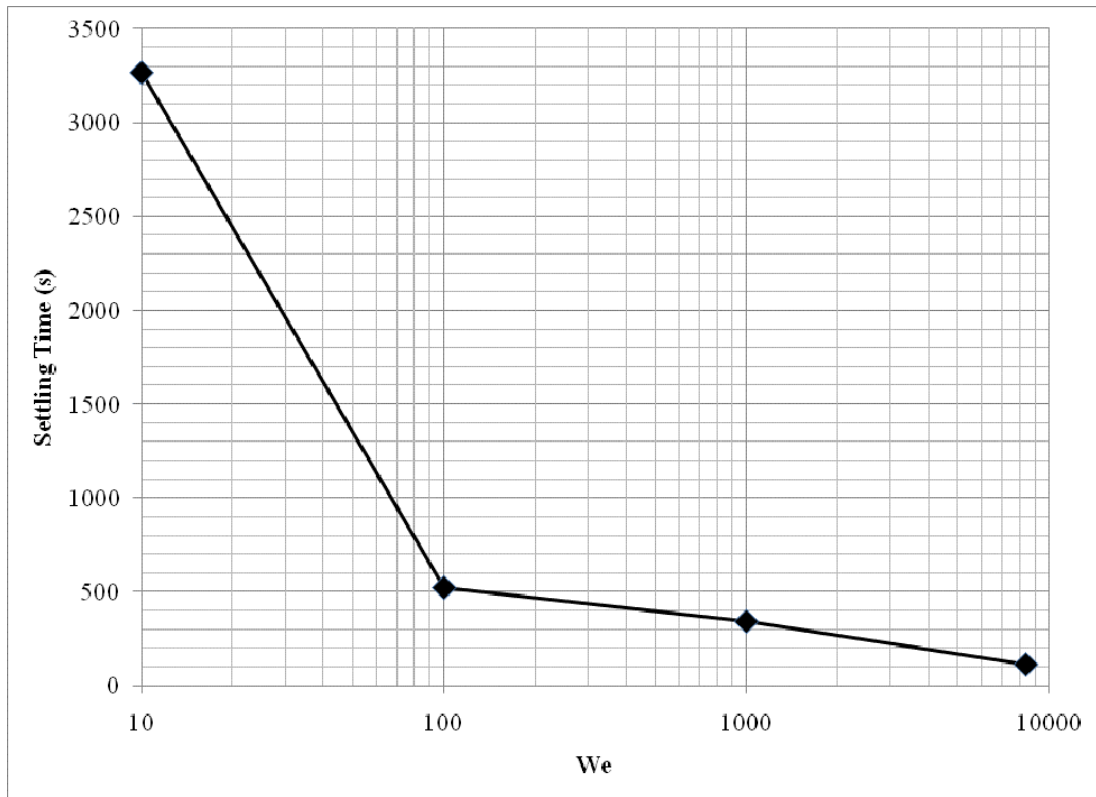


Figure 5.16: Constant Acceleration Settling Time vs. Weber Number

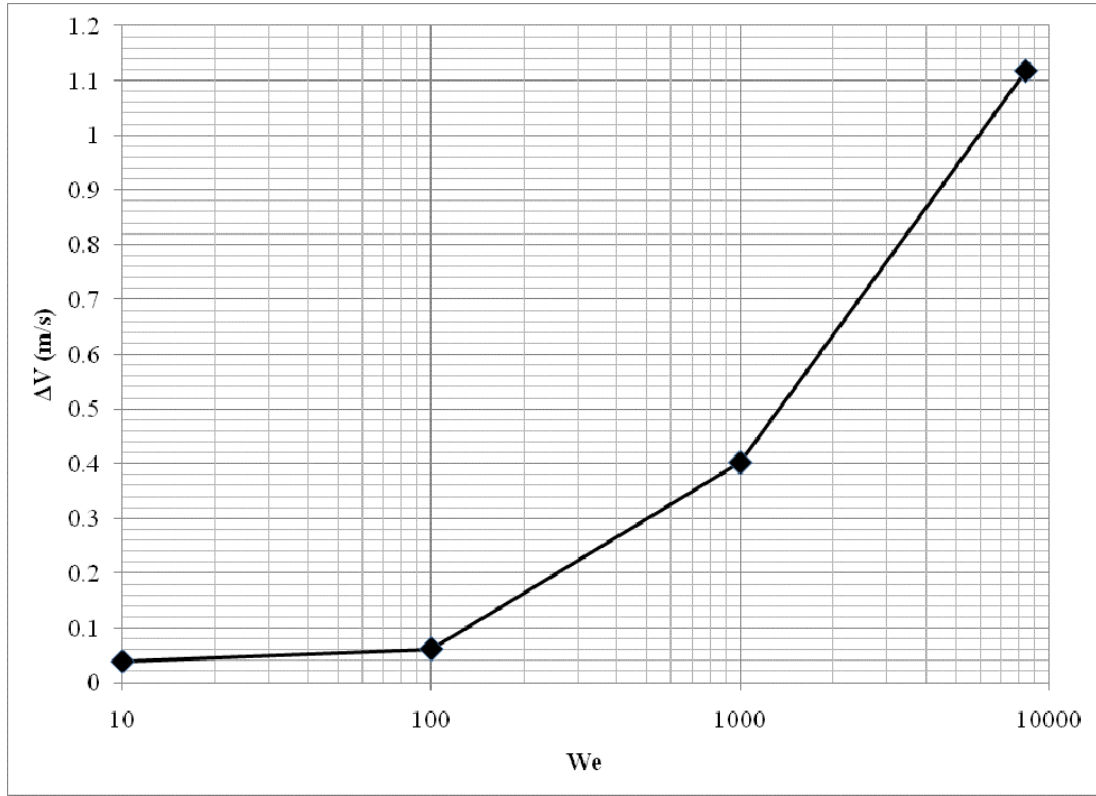


Figure 5.17: Constant Acceleration  $\Delta V$  vs. Weber Number

The plot in Figure 5.17 shows that, for the given architecture, turning on an RCS engine to settle the propellant will cost approximately 1.1 m/s. For this LDS application, there is no time constraint on the settling process, so there is no need to settle the propellant at a higher acceleration when it can be done more efficiently at a lower acceleration. As such, the propellant in this tank, at the 50% fill level, can be settled at the cost of approximately 0.04 m/s by settling at  $We=10$ .

However, the RCS would not be able to throttle down by orders of magnitude to produce a constant acceleration to give Weber numbers of 10 or even 100. This means that the low acceleration cases are not flight-like. This can be remedied by pulsing the RCS thrusters at their nominal thrust level. The thrusters provide 0.001g of acceleration for a specified period of time and are then turned off for a period of time. This creates a time averaged Weber number. Implementation of pulsing into the CFD model will be discussed in Chapter VI along with the pulsed settling analysis.



## CHAPTER VI

### PULSED ACCELERATION ANALYSIS

Analysis for constant acceleration propellant settling was performed for a LDS that showed the propellant could be sufficiently settled with a minimal required  $\Delta V$ . However, this was accomplished at low accelerations that do not correspond to flight-like conditions. This can be remedied by pulsing the RCS for the purpose of creating a time averaged Weber number. Since the constant acceleration analysis was performed for  $We = 10$ ,  $We = 100$ , and  $We = 1000$ , it is desired to perform the pulsed settling analysis for the same three Weber numbers. This will be achieved by turning the RCS on for a period of time and then turning it off. This phenomenon will be referred to as the duty cycle. There is a minimal transient involved for a real system due to valve opening and closing times that are on the order of tens of milliseconds. Resolving this transient would require a maximum time step smaller than that. For this reason and the fact that modeling the transient will not appreciably change the time averaged Weber number, this transient effect will not be modeled in this analysis. Rather, the RCS will provide an acceleration of  $0.001g$  for a period of time and then be turned off completely. This duty cycle will

repeat throughout the simulation. The duty cycle for each Weber number is listed in Table 6.1.

Table 6.1: Duty Cycle for Time Averaged Weber Numbers

Weber Number	Burn Time (s)	Off Time (s)
10	0.02	16
100	0.1	8
1000	1	8

Modeling pulsed acceleration settling is possible in CFD-Ace+ through the use of time dependent gravity. The user creates a text file with gravity as a function of time, and the code reads the value at each time step, linearly interpolating between points. The additional constraint that must be imposed for the  $We = 10$  and  $We = 100$  calculations is the maximum time step. Without a maximum time step imposed for these two cases, it is possible that the code will skip over the burn time part of the duty cycle at various points throughout the simulation. Additionally, the acceleration could be imposed for too long if the time step is too large. Maximum time steps of 0.1 seconds and 0.02 seconds must be imposed for the  $We = 100$  and  $We = 10$  calculations, respectively.

One additional restraint that is important for implementing this strategy for real systems is the zero gravity interface formation time. Given enough time in a zero gravity

environment, the liquid-gas interface will reorient to an equilibrium condition. This is undesirable, and it is necessary to calculate this reorientation time when implementing a pulsed settling acceleration strategy. The reorientation time is calculated from an empirical relation first correlated by Siegert [2]. The relation is given for cylindrical tanks by equation (6.2), in which  $D$  is the tank diameter.

$$t_{orientation} = 0.15\sqrt{\frac{\rho D^3}{\sigma}} \quad (6.1)$$

For this tank, the orientation time was calculated to be approximately 30 seconds. This is assuming the tank is cylindrical, so there could be error associated with this calculation depending on the orientation of the liquid. If the liquid-gas interface is oriented in one of the tank domes, this value could be much smaller than 30 seconds. For this reason, the zero gravity environment was imposed for no more than 16 seconds.

The duty cycle given in Table 6.1 was rounded for simplicity, so there is a small difference between the constant acceleration Weber numbers and the pulsed acceleration Weber numbers. There is additional error caused by the fact that settling occurs in the middle of a duty cycle. This is more important for a case in which the fluid encounters fewer duty cycles, the higher Weber numbers in this case. Table 6.2 shows the desired Weber number and the actual Weber number for the pulsed acceleration cases. The maximum deviation from the desired value is 6%.

Table 6.2: Pulsed Settling Weber Numbers

Desired	Actual
10	10.5
100	106
1000	965

After pulsing was implemented into the CFD model, calculations could be performed. The first comparison to be made between the constant and pulsed settling cases is the progression of the geysers longitudinally through the tank. Figures 6.1 through 6.3 show the geyser progression for the constant and pulsed accelerations for each Weber number.

The primary difference in the geyser progression for the  $We = 1000$  case is seen in Figure 6.1. The geyser for the pulsed settling case progressed further through the tank, causing its maximum progression time to lag the constant acceleration case by about 4 seconds. The geysers are of similar shape, and the fluid dynamic environment within the tank is similar for the two cases.

The most noticeable difference for the  $We = 100$  cases is shown by Figure 6.2. Similar to what happened in the  $We = 1000$  case, the geyser progressed further through the tank in the  $We = 100$  case. Due to the very slow deformation and progression of the geyser for this Weber number, the lag associated with this difference was 20 seconds.

The geyser in the pulsed acceleration case became different in shape as it progressed into the tank ullage.

As was previously discussed, there is no geyser formation for the  $We = 10$  case. In both the constant and pulsed settling cases, a bubble forms when the liquid converges in the tank's aft dome, and this bubble moves about the tank in an oscillatory manner for a period of time with the mean longitudinal CG value slowly decreasing. The primary differences in the dynamics of these cases are better illustrated by the CG plots which will be discussed in detail later in the chapter.

Although the time averaged Weber numbers were designed to closely match the constant acceleration Weber numbers, it is expected that there will be some difference in the CG movement throughout the course of the simulations. Figures 6.4 through 6.6 show the CG movement for each case. The behavior of the tanked  $LH_2$  is similar for each case. The timing and progression of the geysers are the most notable difference. The behavior of the CG of the bulk liquid is similar in each case.

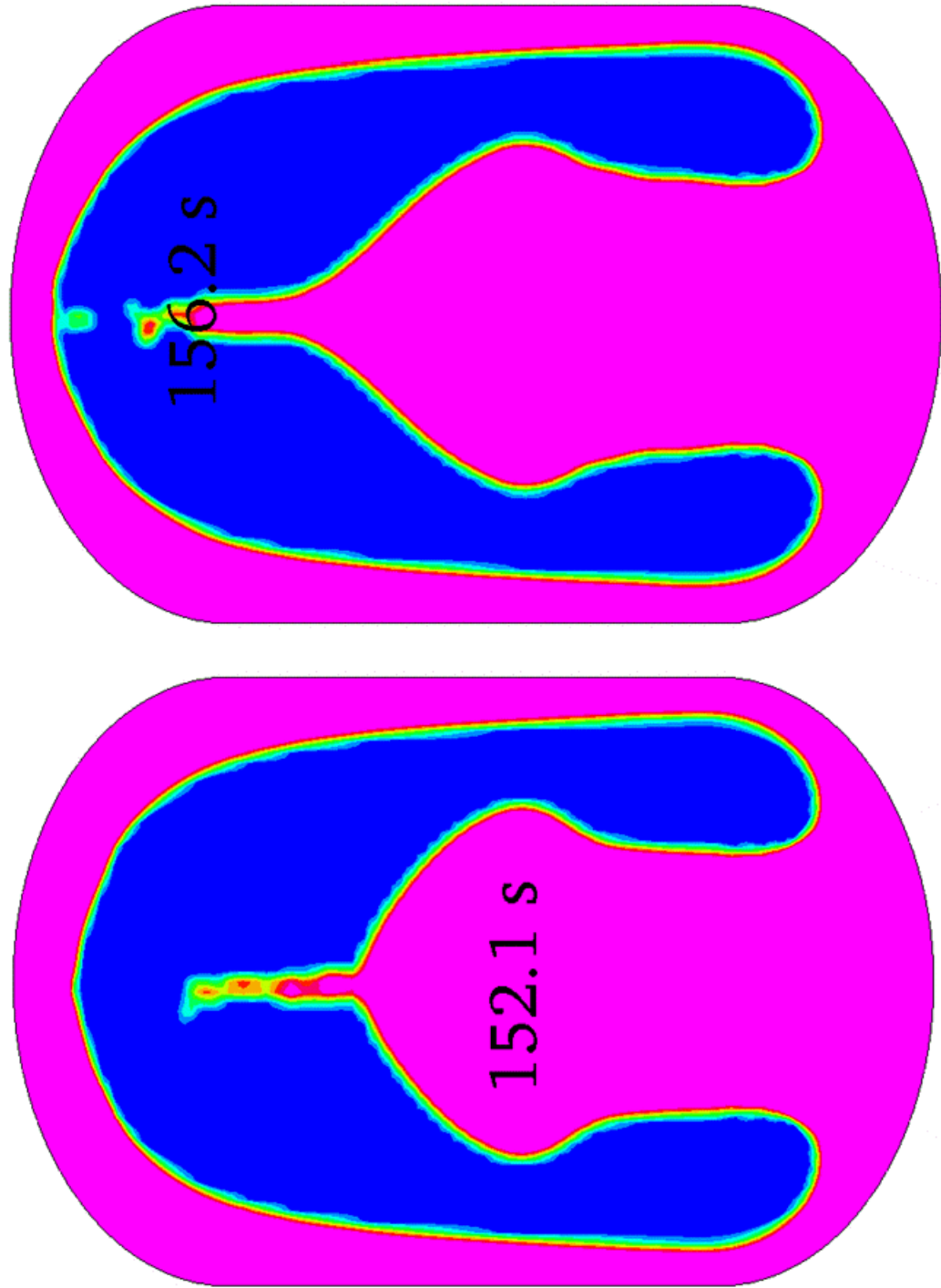


Figure 6.1:  $We = 1000$  Geyser Progression for Constant (bottom) and Pulsed (top) Accelerations

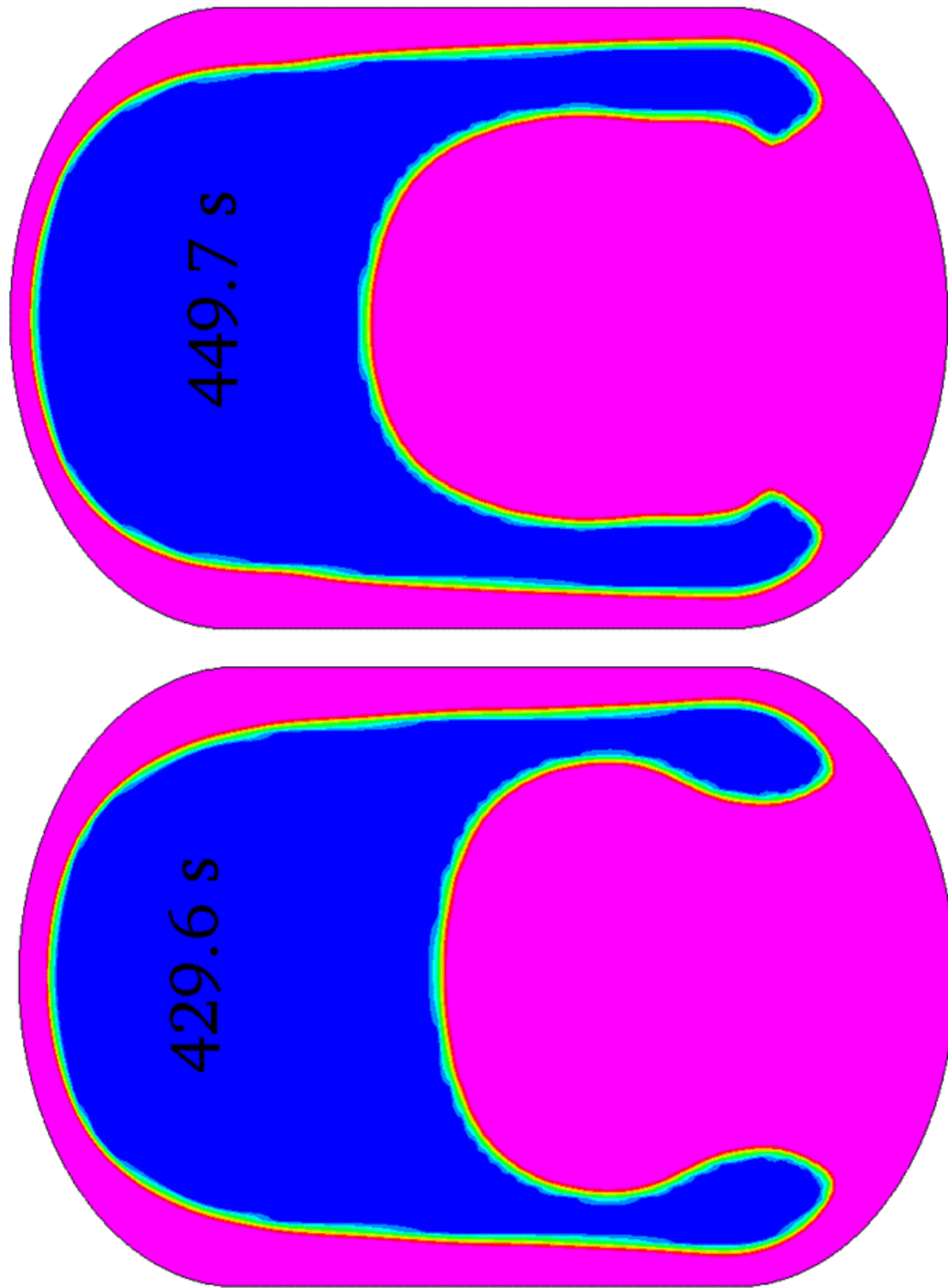


Figure 6.2:  $We = 100$  Geyser Progression for Constant (bottom) and Pulsed (top) Accelerations

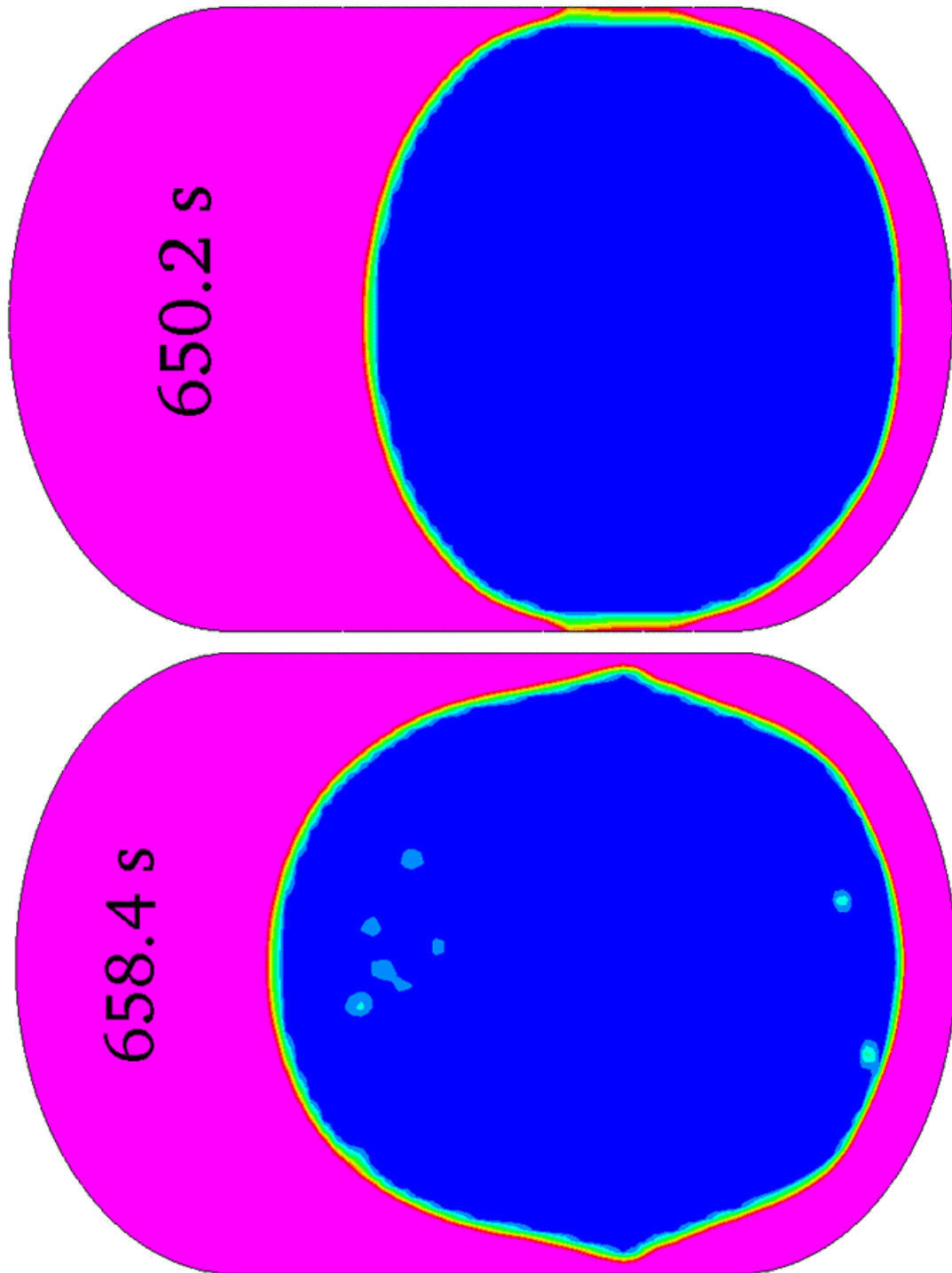


Figure 6.3:  $We = 10$  Geyser Progression for Constant (bottom) and Pulsed (top) Accelerations



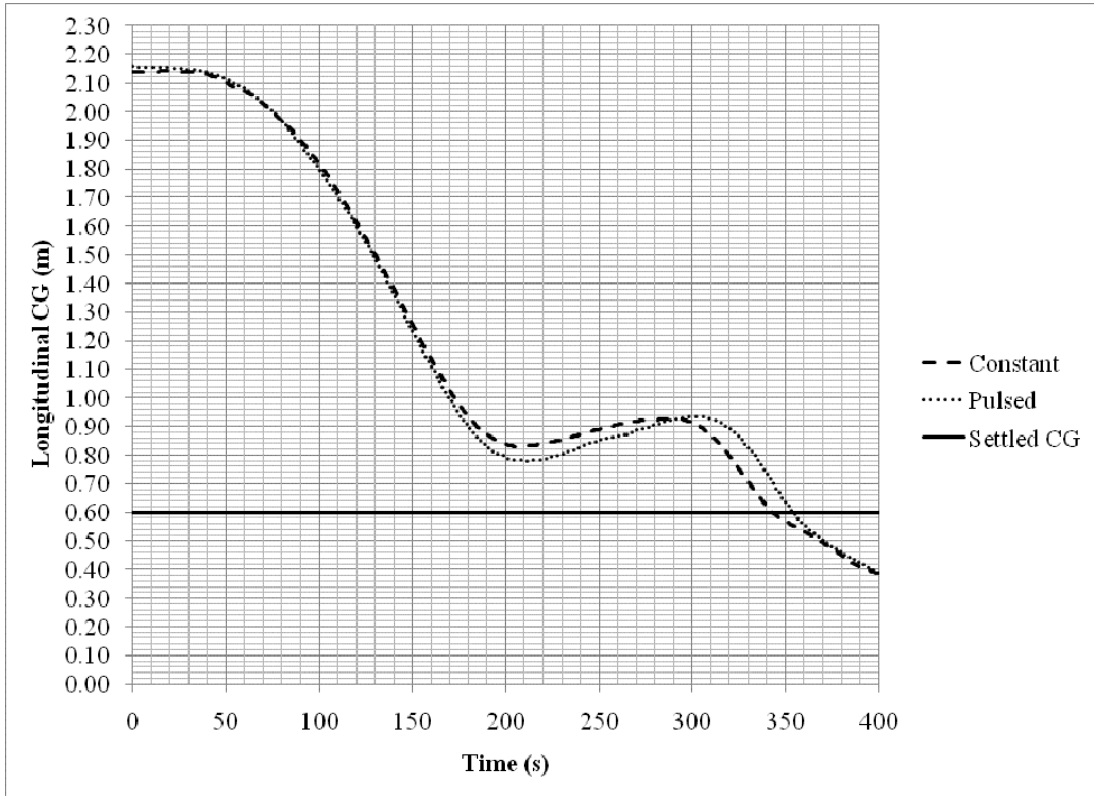


Figure 6.4: CG Plot for  $We = 1000$  Case

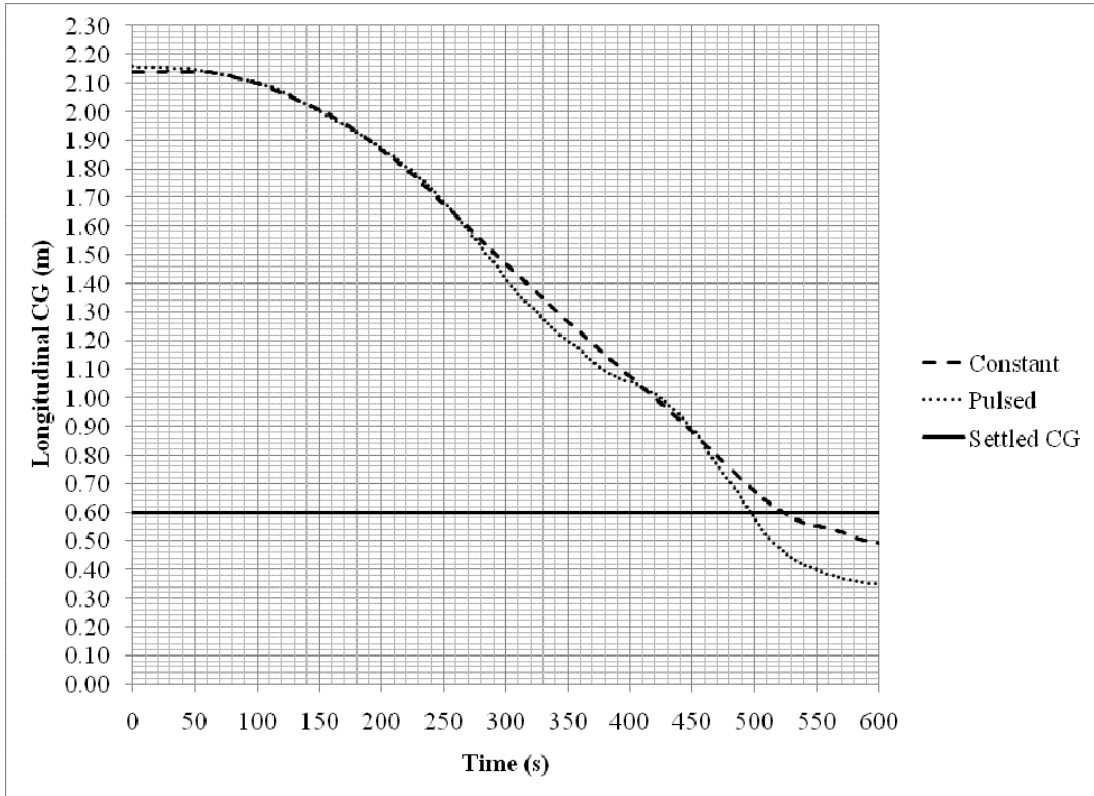


Figure 6.5: CG Plot for  $We = 100$  Case

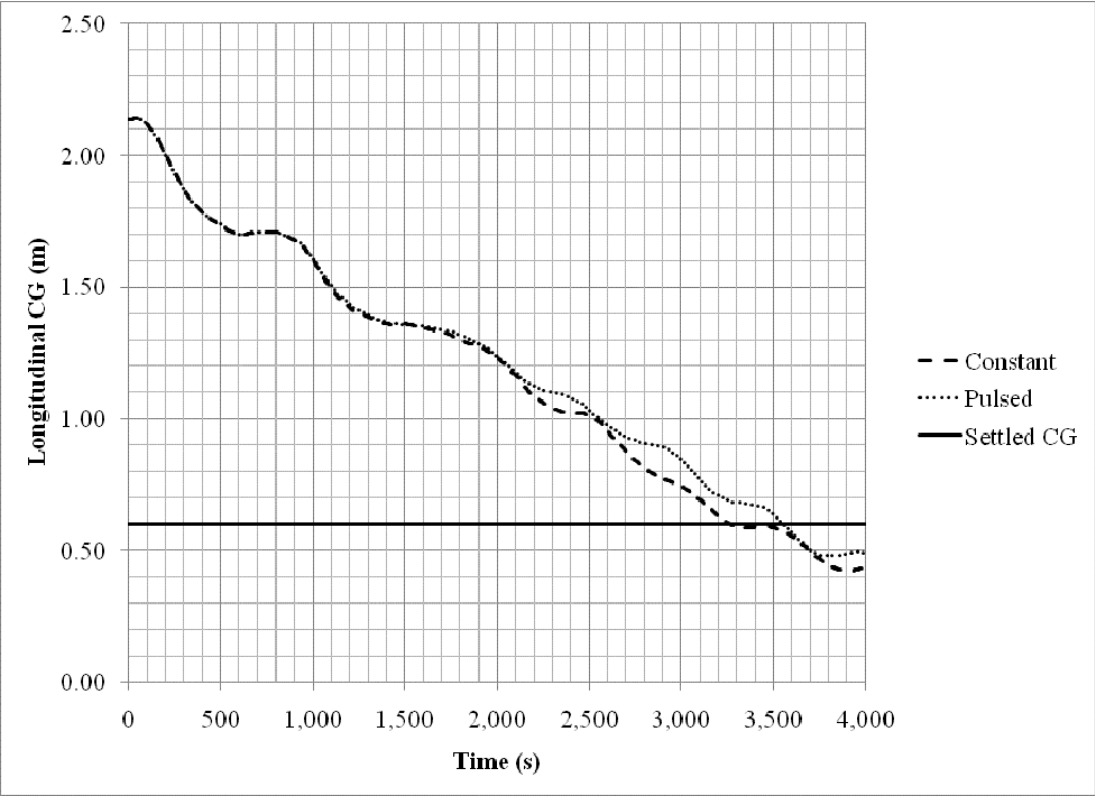


Figure 6.6: CG Plot for We = 10 Case

Figures 6.4 through 6.6 show that the CG of the tanked LH<sub>2</sub> behaves similarly for the constant and pulsed acceleration cases. Settling times are also quite similar, but are summarized in Table 6.3.

Table 6.3: Settling Time Summary for Constant and Pulsed Acceleration Cases

Acceleration or Weber Number	Constant Acceleration	Pulsed Acceleration
0.001g	114	N/A
We = 1000	343	354
We = 100	523	497
We = 10	3264	3556

Table 6.3 shows the settling times for the constant and pulsed acceleration cases. The settling times for the pulsed acceleration cases are similar to the settling times for the constant acceleration cases. Some of the difference is accounted for by the small difference in actual Weber number versus desired Weber number. The only case in which the percent difference between the two settling times falls outside of that range is the We = 10 case, in which the pulsed acceleration settling time differs 9% from the constant acceleration settling time. This difference is too small to qualify by examining images of the liquid volume fraction. However, for the first 2,100 seconds of the simulation, the CG behavior is identical for the pulsed and constant acceleration cases. It

is only after that time that the behavior changes. It is thought that, due to the fact that the propellant is in the tank's aft dome, the zero gravity interface reorientation time is smaller than was calculated by the empirical relation due to the difference in tank geometry. The dynamics of the CG are oscillatory for the small Weber number case, and this seems to be the case when the acceleration is pulsed. It can be seen in Figure 6.6 that the peak to peak oscillations are larger for the pulsed case than for the constant acceleration case.

Settling times for all simulations have been plotted in Figure 6.7, in which markers for the pulsed acceleration cases have been superimposed as white triangles. The corresponding  $\Delta V$  values have been plotted in Figure 6.8.

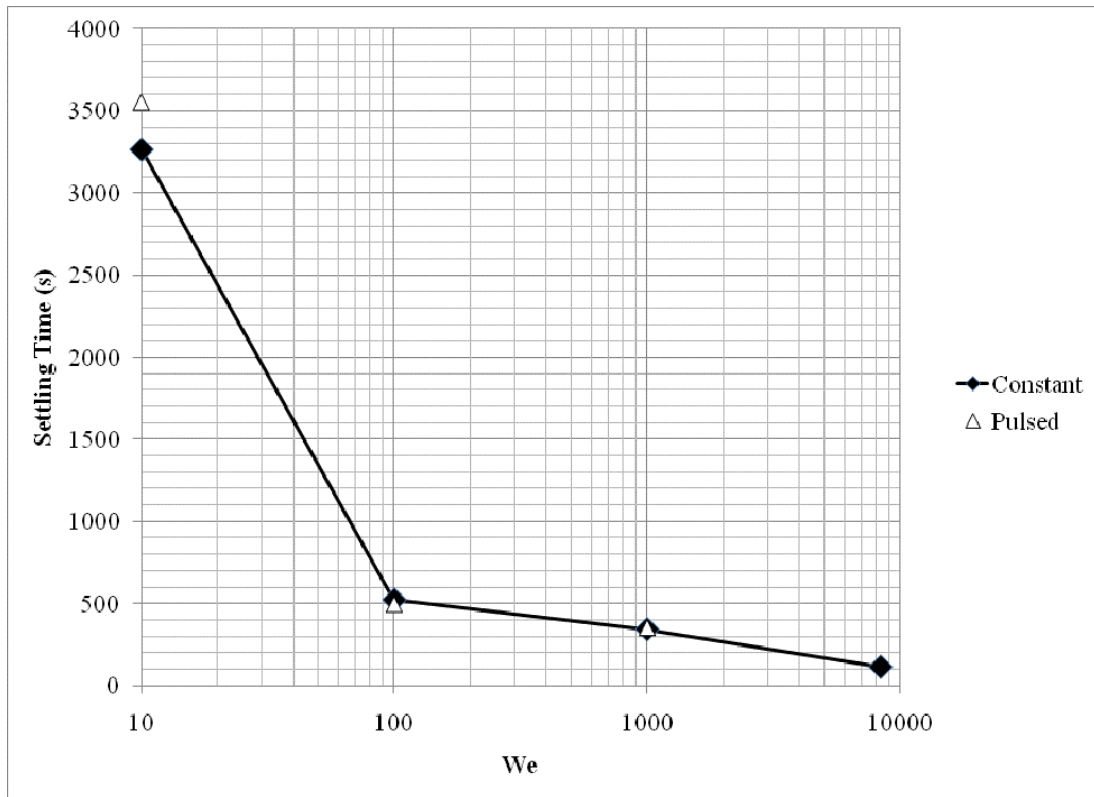


Figure 6.7: Settling Time vs. Weber Number

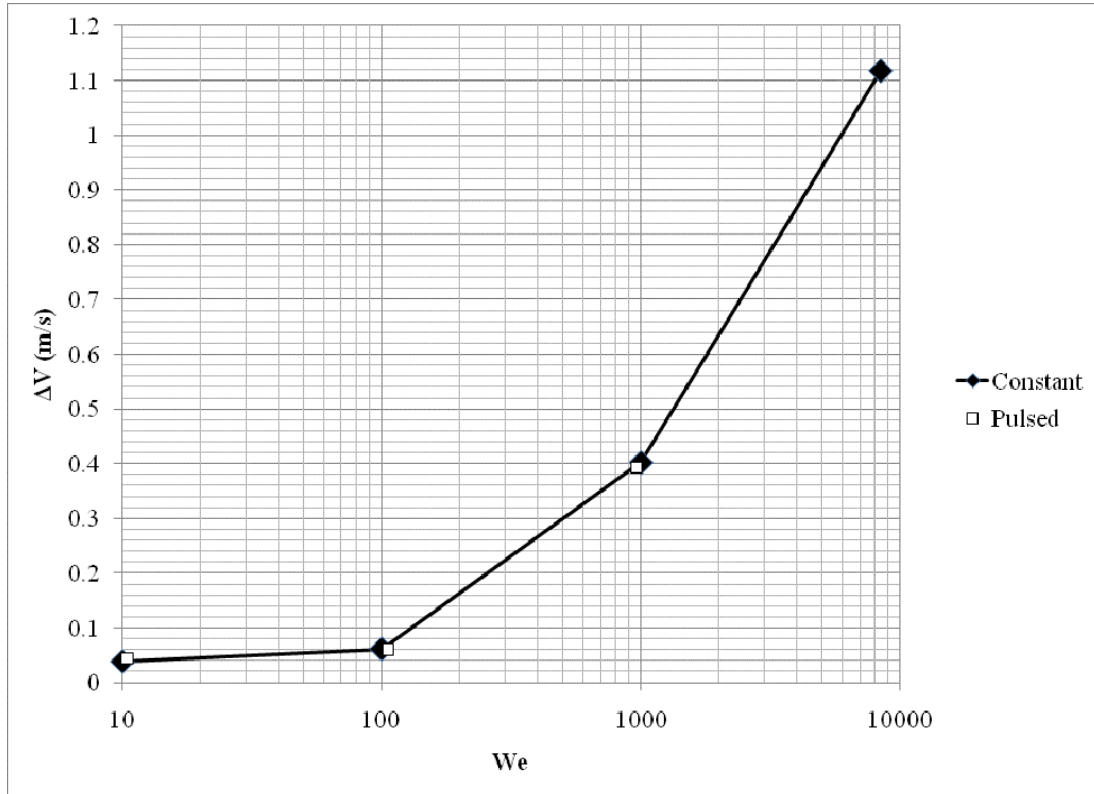


Figure 6.8: Required  $\Delta V$  vs. Weber Number

The largest difference in settling time between the constant and pulsed acceleration cases was seen in the  $We = 10$  case. The pulsing, for the chosen acceleration profile, caused a difference in settling time of 9%. Because the actual Weber number was higher than the desired Weber number, this resulted in a required  $\Delta V$  of about 4.4 cm/s, compared with 3.8 cm/s for the constant acceleration case. This was, by far, the largest difference seen for any of the cases. This LDS configuration can be settled with as little  $\Delta V$  as 5 cm/s, with a margin of over 10%, assuming there are no time constraints on the settling process.



## CHAPTER VII

### CONCLUSIONS

A CFD model was developed for validation against a drop tower test performed at the Zero Gravity Facility at NASA Lewis Research Center. The CFD model produced similar results to the test and it was determined that the CFD model has the ability to capture the necessary dynamics of the propellant settling process. The predictive calculations produced in this thesis were grid and CFL number independent.

A CFD model was developed for a LO<sub>2</sub>/LH<sub>2</sub> Lunar Descent Stage propellant settling scenario. It was determined that settling the Liquid Hydrogen would also settle the Liquid Oxygen, so only the Liquid Hydrogen scenario was studied. Constant accelerations were applied to the liquid to simulate Weber numbers of 8,400; 1,000; 100; and 10. The most efficient settling design, given constraints on the settling time, was the  $We = 10$  case. Because typical Reaction Control System thrusters cannot throttle down by orders of magnitude, the lower Weber numbers are not flight-like. A pulsed acceleration strategy was implemented in order to create a time averaged Weber number that matched the desired value. This pulsing was able to settle the propellant in a similar time with a similar required  $\Delta V$ . Similar to the constant acceleration cases, the

$We = 10$  case gave the best performance. It is desirable to settle the propellant, by pulsed acceleration, at a Weber number of about 10.

CFD analysis of the propellant settling process is important. Liquid rocket engines will continue to be used for many different applications that require an in-flight engine start or tank vent in a microgravity scenario. These applications include descent stages, stages similar to the Ares V Earth Departure Stage or Saturn S-IVB third stage, in-space rendezvous, and orbital maneuvers.

APPENDIX

AIAA JOURNAL OF PROPULSION AND POWER ARTICLE

Josh Rojahn

Georgia Richardson, Ph. D.

The University of Alabama in Huntsville

## A. 1. INTRODUCTION

The primary goal of this paper is to numerically optimize, using a computational fluid dynamic (CFD) analysis tool, the propellant settling process in a generic Lunar Descent Stage liquid hydrogen (LH<sub>2</sub>) tank. It is necessary to settle the liquid to the bottom of the tank so the tank can be vented or the engine can be started without any ullage gas being ingested into the propellant feed line. To perform this settling maneuver, some sort of auxiliary propulsion system, usually a Reaction Control System, must be fired to provide a downward acceleration on the liquid propellants. This required thrust costs mass, and it will be the goal of this study to minimize that mass by minimizing the required change in velocity ( $\Delta V$ ).

This analysis will study the propellant settling process over a wide range of acceleration levels, and it is more instructive to do so by discussing the variables in terms of the dimensionless Weber number. The Weber number is defined as the ratio of inertial forces to surface tension forces, and is given by the following equation, in which  $V$  is the characteristic velocity [2].

$$We = \frac{\rho V^2 R}{\sigma} \quad (\text{A.1})$$

The velocity in the Weber number is calculated by using the following semi-empirical relation for the velocity of the flow as it impacts the tank bottom, in which  $x_L$  is the distance from the liquid-gas interface to the tank bottom [3].

$$V = \sqrt{1.8ax_L} \quad (\text{A.2})$$

## **A. 2. ANALYSIS TOOL**

The CFD code used for this analysis is CFD-Ace+, a finite volume method code that utilizes the Volume of Fluid (VOF) algorithm to account for the liquid-gas interface. The code also accounts for the surface tension forces that exist at the interface. This code uses a structured, body fitted grid methodology. A special user subroutine was implemented to track the time history of the liquid propellant center of gravity (CG).

## **A. 3. ANALYSIS APPROACH AND METHODOLOGY**

The goal of this thesis is to minimize the  $\Delta V$  required for settling a liquid propellant in a flight-like tank. Due to the variability in possible designs for a LDS, there are many possible tank geometries. However, analysis will be conducted based on the Weber number, a dimensionless parameter that contains information about the tank geometry, propellant fill level, fluid properties, and vehicle acceleration. The tank analyzed in this thesis will be a 28.32 m<sup>3</sup> (1000 ft<sup>3</sup>) cylindrical LH<sub>2</sub> tank with 1/√2 ellipsoidal, convex end caps. The tank radius was chosen to be 1.52 m (5 ft), requiring a tank barrel length of 2.44 m (8 ft). The tank geometry for this LDS is shown below in Figure A.1.

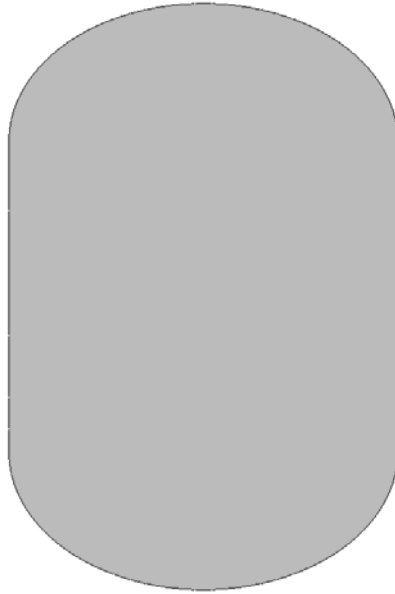


Figure A.1: LDS Tank Geometry

Due to the long duration of microgravity coast between Low Earth Orbit and the Moon, the worst case initial condition will be imposed for the LH<sub>2</sub> propellant. That is, all of the propellant will be located in the top of the tank with a quiescent surface. The tank will be half full with LH<sub>2</sub> for this analysis. The ullage will be helium, a common pressurant gas used for liquid propellant tanks. Because heat transfer is not being taken into consideration, both ullage gas and liquid will be treated as incompressible with constant fluid properties.

Prior to conducting the analysis, a condition must be defined at which the propellant is deemed to be sufficiently settled. Since the longitudinal CG of the liquid propellant will be tracked throughout the simulation, the propellant will be deemed to be settled when the value of the CG crosses some threshold value. Each simulation will be performed with the goal of determining one threshold value that is adequate for all

four cases. The four cases are 0.001g acceleration and Weber numbers of 10; 100; and 1,000. After post-processing each simulation, it was found that an appropriate threshold value was 0.6 m above the bottom of the tank's barrel section.

Model validation was performed in addition to solution verification. Solution verification activities included a grid convergence study to ensure that settling times were independent of grid resolution. Additionally, a CFL sensitivity study was performed.

Seven cases in total were simulated in the test tank, which was 50% full with LH<sub>2</sub> with Helium ullage gas. Each acceleration or Weber number was simulated at constant acceleration. However, due to the throttling limitations, the smaller Weber numbers cannot be achieved in a flight-like scenario. However, the RCS can be pulsed on and off to create a time averaged acceleration, and thus, a time averaged Weber number. Weber numbers of 10; 100 and 1000 were simulated using a pulsed acceleration strategy. Pulsed acceleration cases cannot perfectly match the constant acceleration Weber numbers, but the came within  $\pm 6\%$ . The propellant was never subjected to a zero gravity environment for more than 16 seconds in any of the cases, so the interface reorientation time [2] was never reached.

#### **A. 4. PROPELLANT SETTLING ANALYSIS**

The parameter of concern for this analysis is the CG of the bulk liquid, which has been tracked throughout the simulation for both constant and pulsed acceleration cases. The CG time histories are plotted for each acceleration in Figures A.1-A.4.

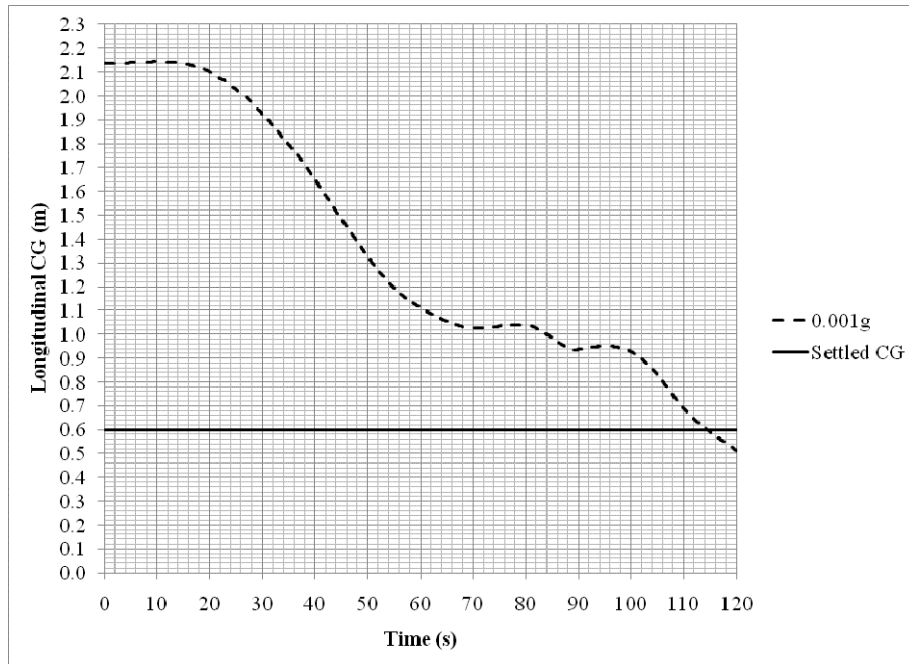


Figure A.2: CG Plot for 0.001g Acceleration Case

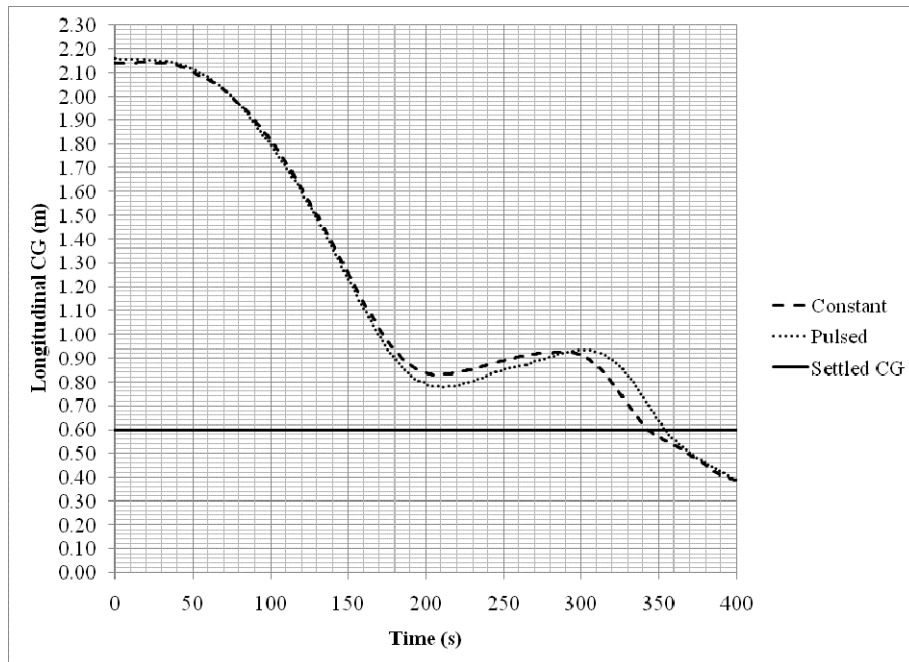


Figure A.3: CG Plot for We = 1000 Case



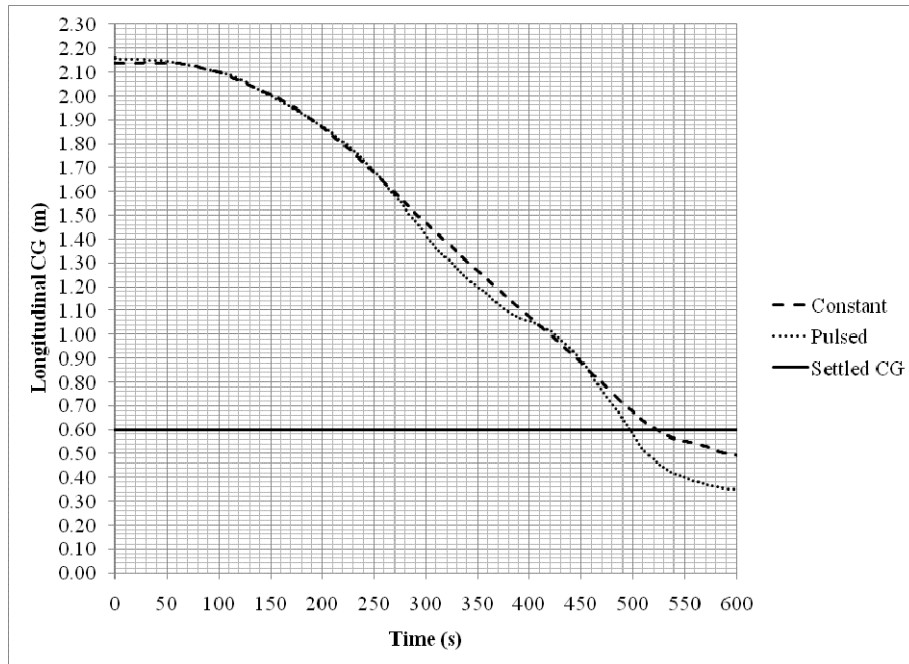


Figure A.4: CG Plot for We = 100 Case

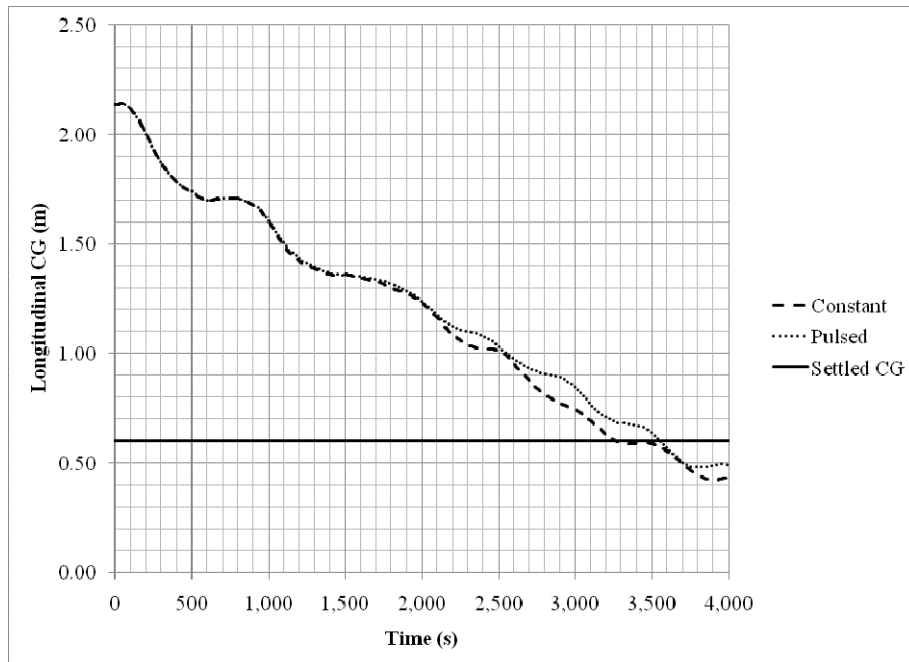


Figure A.5: CG Plot for We = 10 Case

Figure A.6 plots the settling times for the constant and pulsed acceleration cases. The settling times for the pulsed acceleration cases are similar to the settling times for the constant acceleration cases. Some of the difference is accounted for by the small difference in actual Weber number versus desired Weber number. The only case in which the percent difference between the two settling times falls outside of that range is the  $We = 10$  case, in which the pulsed acceleration settling time differs 9% from the constant acceleration settling time.

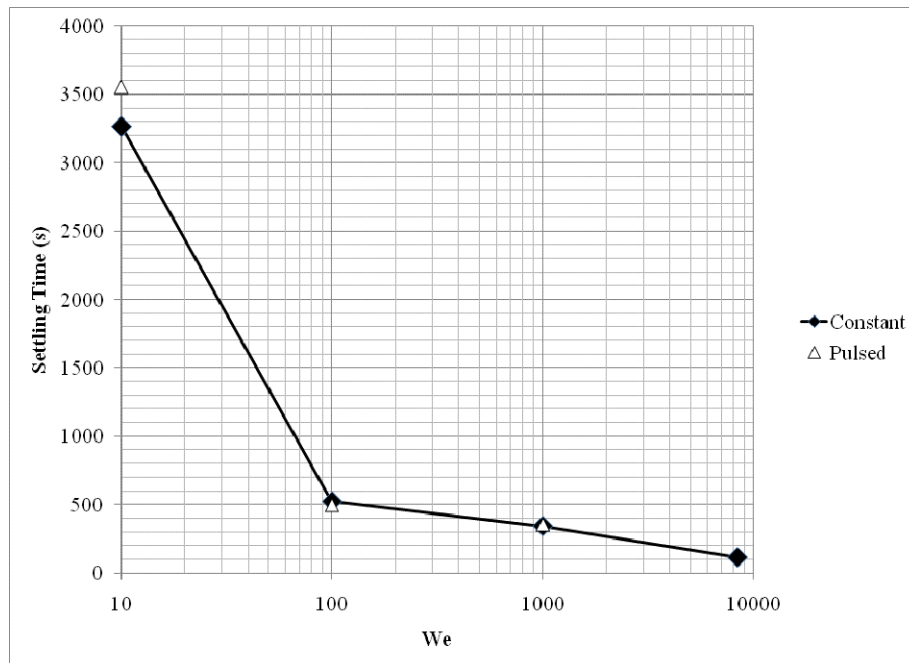


Figure A.6: Settling Time vs. Weber Number

Figure A.6 shows the trend of decreasing settling time with increasing Weber number. However, the goal of this study is to minimize the required  $\Delta V$  for propellant settling. This parameter has been plotted in Figure A.7.

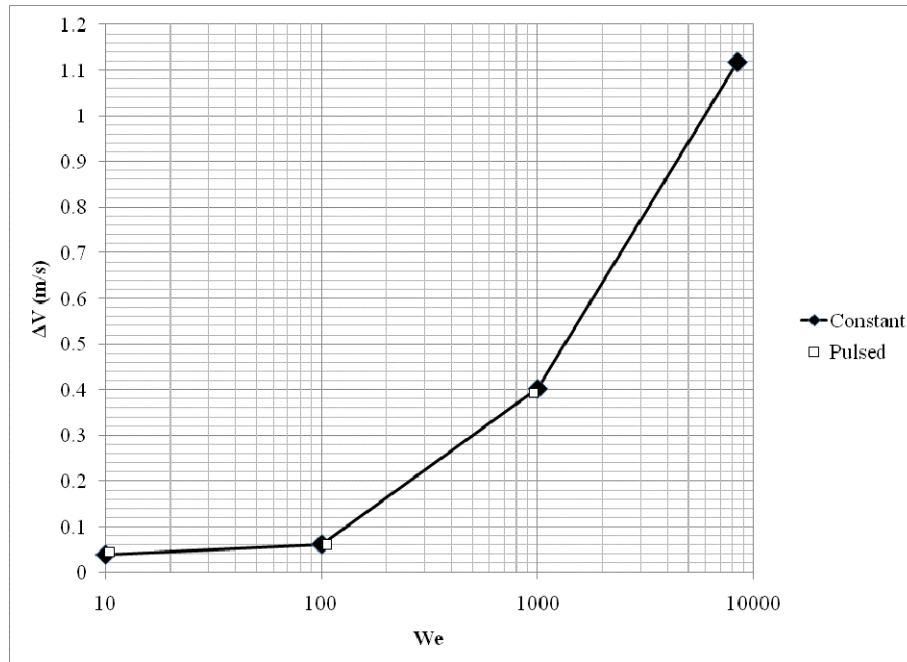


Figure A.7: Required  $\Delta V$  vs. Weber Number

As is shown by Figure A.7, required  $\Delta V$  increases with Weber number. The most efficient settling occurs at Weber numbers between 10 and 100 and can be achieved with as little as 0.05 m/s of  $\Delta V$ .

## A. 5. CONCLUSIONS

A CFD model was developed for propellant settling in a liquid hydrogen Lunar Descent Stage propellant tank. Both constant and pulsed acceleration settling was simulated with the CFD model. Behavior of the liquid CG was very similar for constant and pulsed settling. It is desirable to settle the propellant, by pulsed acceleration, at a Weber number of about 10, but the process is also very efficient at Weber numbers up to 100.

## REFERENCES

- [1] P. Tipler and G. Mosca, "Physics for Scientists and Engineers," W.H. Freeman and Company, 2008
- [2] F. Dodge, "The New 'Dynamic Behavior of Liquids in Moving Containers'," Southwest Research Institute, 2000
- [3] J.A. Salzman, W.J. Masica and R.F. Lacovic, "Low-Gravity Reorientation in a Scale-Model Centaur Liquid-Hydrogen Tank," NASA TN-D 7168, 1973
- [4] I.E. Sumner, "Liquid Propellant Reorientation in a Low-Gravity Environment," NASA TM-78969, 1978
- [5] J.I. Hochstein, A.E. Patag and D.J. Chato, "Modeling of Impulsive Propellant Reorientation," NASA TM 101440, 1989
- [6] A.E. Patag, J.I. Hochstein and D.J. Chato, "Modeling of Pulsed Propellant Reorientation," NASA TM 102117, 1989
- [7] CFD-Ace+ V2009.0 Modules Manual Part 1, ESI Group, 2008
- [8] CFD-Ace+ V2009.0 User Manual, ESI Group, 2008
- [9] CFD-Ace+ V2009.0 Modules Manual Part 2, ESI Group, 2008